JOURNAL OF GEOPHYSICAL RESEARCH, VOL. 99, NO. C2, PAGES 3373–3392, FEBRUARY 15, 1994

Estimates of particle- and thorium-cycling rates in the northwest Atlantic Ocean

R. J. Murnane
Program in Atmospheric and Oceanic Sciences, Princeton University, Princeton, New Jersey

J. K. Cochran
Marine Sciences Research Center, State University of New York at Stony Brook

J. L. Sarmiento
Program in Atmospheric and Oceanic Sciences, Princeton University, Princeton, New Jersey

Abstract. We provide least squares estimates of particle-cycling rate constants and their errors at 13 depths in the Northwest Atlantic Ocean using a compilation of published results and conservation equations for thorium and particle cycling. The predicted rates of particle aggregation and disaggregation vary through the water column. The means and standard deviations, based on lognormal probability distributions, for the lowest and highest rates of aggregation (β_2) and disaggregation (β_{-2}) in the water column are $8\pm27\ y^{-1} < \beta_2 < 18\pm90\ y^{-1}$, and $580\pm2000\ y^{-1} < \beta_{-2} < 3\times10^3\pm10^4\ y^{-1}$. Median values for these rates are $2.1\ y^{-1} < \beta_2 < 3.2\ y^{-1}$, and $149\ y^{-1} < \beta_{-2} < 156\ y^{-1}$. Predicted rate constants for thorium adsorption ($k_1 = 5.0\pm1.0\times10^4\ m^3\ kg^{-1}\ y^{-1}$) and desorption ($k_{-1} = 3.1\pm1.5\ y^{-1}$) are consistent with previous estimates. Least squares estimates of the sum of the time dependence and transport terms from the particle and thorium conservation equations are on the same order as other terms in the conservation equations. Forcing this sum to equal zero would change the predicted rates. Better estimates of the time dependence of thorium activities and particle concentrations and of the concentration and flux of particulate organic matter would help to constrain estimates of β_2 and β_{-2}.

Introduction

Thorium is one of the elements most affected by particle cycling in the ocean because it is rapidly adsorbed onto particle surfaces [*Jannasch et al.*, 1988; *Moore and Millward*, 1988]. Previous workers used thorium isotopic data from the field to infer a range of adsorption and desorption rates of thorium onto and off of particles in the ocean [*Bacon and Anderson*, 1982; *Bacon et al.*, 1985; *Nozaki et al.*, 1987]. Our interests focus on the information thorium can provide about particle cycling. For example, the increase with depth of ^{230}Th in both solution and suspended particle phases [*Bacon and Anderson*, 1982] coupled with the observation of seasonality in thorium fluxes [*Bacon et al.*, 1985] requires the existence of two classes of particles that interact in the ocean: small particles that are slow or nonsinking and large particles that sink at velocities on the order of 10^2 m d^{-1}. Observations such as these have shaped paradigms about the biogeochemical cycle of particles in the ocean.

Ideally, we want to use the distribution of thorium isotopes among the dissolved phase and particle classes to estimate the rates and the efficiency of nutrient and carbon transport through the ocean. This is not a new aspiration. For example, *Eppley* [1989] suggested that the flux of ^{234}Th out of the mixed layer could be used to estimate new production, and *Coale and Bruland* [1987] showed that thorium scavenging rates varied as a function of new production rather than total production. However, clear interpretations of sediment trap results and thorium budgets have proven to be difficult (e.g., [*Buesseler*, 1991]), and the goal of using thorium fluxes as a proxy for new production has yet to be achieved.

The rate of particle interactions through the water column has implications for the dynamics of deep ocean nutrient remineralization. The wide range in estimated thorium- and particle-cycling rate constants (Table 1) suggests that either our interpretation of particle and thorium data may need improvement or that there is significant natural variability. Several possibilities could explain the variability (or discrepancy?) between different sets of flux or rate estimates. One possibility is that inappropriate assumptions are being made when analyzing the data (e.g., it may be that a system is not at steady state and that advective and/or diffusive transport could be important). Another possibility is that despite the different parent distributions and half-lives of the thorium isotopes, thorium isotope data cannot constrain the fluxes and cycling rates of nutrients or particles (i.e., more independent data are needed). Better estimates of the particle-cycling rate constants and of the errors associated with the rates are needed if we are to address these possibilities and use thorium data to constrain nutrient and carbon cycling in the ocean.

In this paper we present a least squares analysis of thorium isotopic and particle data from the Nares Abyssal Plain in the northwest Atlantic. Our goals are as follows: (1) to determine the values and estimate the errors for thorium- and particle-cycling rates as a function of depth through the water column, (2) to ex-

Paper number 93JC02378.
0148-0227/94/93JC-02378$05.00

Table 1. Comparison of Rate Constants

Source	Site	k_1, 10^4 m^{-3} kg^{-1} y^{-1}	k_1', y^{-1}	k_{-1}, y^{-1}	β_{-1}, y^{-1}	β_2, y^{-1}	
Lavelle et al. [1991]	Puget Sound	69±6 – 280±10		316		50±3 – 90±20	
Nozaki et al. [1987] (particulate data)	Western Pacific		0.20±0.27 – 0.44±1.2	0.9±1.2 – 1.9±5.1		2.4±5.9 – 10±210	
Nozaki et al. [1987] (total data)	Western Pacific					0.18	
	Western Pacific					0.14±0.01	
Nozaki et al. [1987] (total + particulate)	Western Pacific					0.11±0.03	
Bacon et al. [1989]	Arctic Ocean	8.7 – 5	0.16 – 0.47	2.6 – 9.8			
Bacon and Anderson [1982]	Panama Basin		0.2 – 1.3	1.3 – 6.3			
Nozaki et al. [1981]	Pacific Ocean		1.5	6.3			
Clegg et al. [1991]	equatorial Pacific	~7 – ~70	1 – 4	2.5±1.0	<0.4 – ~75	<0.1 – ~50	<
	North Pacific		3 – 70			<1 – ~40	
Clegg and Whitfield [1991]		2.3	0.2 – 2.6	1.8	0.03 – 50	4 – 640	1
Murnane et al. [1990]	North Pacific		0.5±0.1	1.0±0.1		0.2±0.01	
Murnane [1993]	North Pacific		0.7±0.4	1.7±0.9		0.8±0.9	
This work		5.0±1.0		3.1±1.5	$4 - 10^3$	8 - 18	5

When β_{-1} is not determined, its action is subsumed into the rate constant k_{-1}. Note (1), rate constants are calculated with a 100 m d^{-1} settling velocity for based on ^{234}Th analyses. Here, k_{-1} is set at 10^{-5} s^{-1} and k_1 is determined from *Lavelle et al.*'s [1991] best fit values of k_1/k_{-1}. This formulation neglects the p to the release of thorium to the dissolved phase. Actual value for β_2 is found from k_3C_s, where C_s is the concentration of large particles (marine snow) and errors were calculated using a "jackknife" statistical technique. Note (2), rate constant data based on ^{230}Th data from filtered particulates at stations AN-1 standard deviation. Note (3), total data rates are found using total ^{230}Th data. Data are from station AN-1. Top row numbers are based on slope and interc *al.* [1987]. Bottom row numbers calculated using data picked from Figure 3 of *Nozaki et al.* [1987]. Errors are equal to one standard deviation. Smaller e rate constants are mostly caused by the greater number of data points relative to filtered particulate data set. Note 4, rate constants and errors are based on from *Nozaki et al.*'s [1987] Figure 3 and particulate data. Larger errors for both rate constants are caused by a greater uncertainty in slope based on a com value for β_{-2} is from a larger calculated intercept. Errors are one standard deviation. Note 5, top row data are based on equatorial Pacific ^{234}Th and particl estimates are based on ^{228}Th, ^{230}Th, and ^{234}Th data from the North Pacific. Negative solutions for rate constants are omitted from ranges. Errors generally are based on synthetic particle profiles and extant data. Note 7, rates are calculated using ^{228}Th, ^{230}Th, and ^{234}Th data and the Wolberg least squares techni calculated using *Tarantola and Valette*'s [1982] total inversion technique. The data were the same as that of *Murnane et al.* [1990]. Rate constants and la were assigned a lognormal probability distribution. Mean and standard deviations are for a lognormal probability distribution. Note 9, for k_1 and k_{-1} the v standard deviation for a lognormal probability distriubtion. The range of rates for β_{-1}, β_2, and β_{-2} give the high and low means (for a lognormal probability water column.

amine the importance of the time dependence and transport terms in the conservation equations for thorium and for particles, and (3) to suggest additional data that could improve the estimates of the particle-cycling rate constants and large-particle concentration. We first outline the thorium and particle cycles that are used in the inversion and in a forward model, then follow with a summary of the field data that are used in the inversion. The least squares estimates for the rate constants predicted with the data and an analysis of the residual terms are then presented. Next, the forward model is used to examine the sensitivity of thorium and particle profiles to different rate constants. Finally, using results of the sensitivity tests, we recommend additional measurements that could help to constrain further the particle-cycling rate constants.

Thorium- and Particle-Cycling

The paradigm for thorium cycling that we use partitions thorium into a dissolved phase and two particle phases (Figure 1a) [*Bacon et al.*, 1985; *Nozaki et al.*, 1987]. One particle phase represents suspended or slowly sinking particles, and the other represents rapidly sinking, large particles. The different phases are operationally defined by sample collection methods and the two particle classes are consistent with analyses of particle size spectra and flux data [*Clegg and Whitfield*, 1990]. Thorium in the dissolved phase is sampled by passing seawater through a filter, thorium in the small-particle phase is associated with material collected by the filter, and thorium in the large-particle phase is determined from material collected by sediment traps. Although colloidal aggregation, or Brownian pumping, appears to be an important component of thorium cycling [*Honeyman and Santschi*, 1989], we will not explicitly include it in this discussion. However, colloidal aggregation is implicitly included in the model by the relatively small rate constant for thorium adsorption compared with laboratory studies of adsorption rate constants [*Jannasch et al.*, 1988; *Moore and Millward*, 1988].

The forward and inverse models of particle and thorium cycling at the Nares Abyssal Plain divide the water column into 13 layers. The 13 layers increase in thickness from 50.9 m at the surface to 1000 m at the bottom, and the top two layers represent the euphotic zone (Table 2). The thickness of the top 12 layers matches those used in a general circulation ocean model of the global ocean phosphate and oxygen cycle [*Najjar et al.*, 1992]. The bottom layer was added so that the total depth in the model was in closer agreement with the depth at the Nares Abyssal Plain. The different depth intervals are shown by bars on the right side of the graphs in Figures 2 and 3.

Model

The behavior of a tracer in the water column is described by the conservation equation

$$\frac{\partial(\ )}{\partial t} = -\vec{\mathbf{V}}\cdot\vec{\nabla}(\ ) + \vec{\nabla}\cdot\mathbf{K}\vec{\nabla}(\ ) + \mathrm{SMS}(\ )$$

For our purposes, ( ) denotes the activity of a thorium isotope or the concentration of a particle phase, and SMS are the source minus sink terms (Figure 1; see Appendix A for detailed equations). The velocity field is given by **V**, the eddy diffusivity by **K**, and time by t. The time rate of change term and the transport terms generally are not known. We combine them into a single term of the form

$$\mathrm{T}(\ ) = \frac{\partial(\ )}{\partial t} + \vec{\mathbf{V}}\cdot\vec{\nabla}(\ ) - \vec{\nabla}\cdot\mathbf{K}\vec{\nabla}(\ )$$

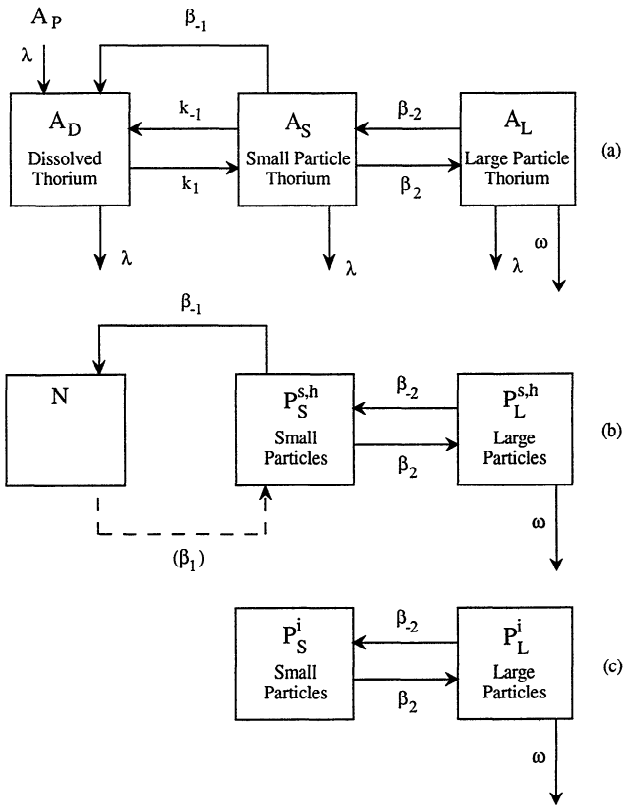

Figure 1. Schematic diagram of the cycling of (a) thorium, (b) soft biogenic and hard biogenic material, and (c) inert detrital material. Thorium activity is divided between the dissolved phase (A_D), suspended small particles (A_S), and sinking large particles (A_L). The large particles sink with a velocity ω. Radioactive decay in each phase is denoted by λ, and the dissolved parent is denoted by A_P. Particle concentrations are given by P. The subscripts S and L denote small and large size classes, respectively. The superscripts denote soft biogenic material (s), hard biogenic material (h), and inert detrital material (i). Biogenic material is formed in the euphotic zone. Nutrient concentrations are given by N. Inorganic adsorption occurs at a rate proportional to $k_1 P_S^t$, where k_1 is the second-order rate constant for inorganic adsorption of thorium (cubic meters per kilogram per year), and P_S^t is the total small-particle concentration. The first-order rate constant for inorganic desorption of thorium is k_{-1}. The first-order aggregation rate constant is β_2, and the first-order disaggregation rate constant is β_{-2}. The first-order rate constant for the formation of biogenic material in the euphotic zone is β_1. Soft biogenic material in the small-particle phase can be remineralized; the first-order rate constant for this process is β_{-1}. Thorium is also released from the small-particle phase to the dissolved phase when soft biogenic material is remineralized at a rate that is proportional to $\beta_{-1} P_S^s$.

such that T( ) = SMS( ). This form of the conservation equation for each tracer at every depth is used as a constraint in the inversion (Appendix A).

The SMS terms for model tracers in each phase are based on the interactions in Figure 1 and fully described in Appendix A. We first discuss the processes affecting thorium. There is exchange of thorium between the dissolved and small-particle phases and the small- and large-particle phases. The adsorption and desorption of thorium onto and off of small particles (k_1 and

Table 2. Initial Estimates of Thorium and Radium Activity

Depth, m	Layer Thickness, m	Dissolved ^{228}Ra, dpm m^{-3}	Dissolved ^{230}Th, dpm m^{-3}	Dissolved ^{228}Th, dpm m^{-3}	Small-Particle ^{234}Th, 10^6 dpm kg^{-1}	Small-Particle ^{230}Th, 10^3 dpm kg^{-1}	Small-Particle ^{228}Th, 10^3 dpm kg^{-1}	Large-Particle ^{228}Th, 10^3 dpm kg^{-1}
25.5	50.9	3.0	0.07	12	-	1.0±0.1	22.0±3.1	16
85.1	68.4	2.5	0.09	12	-	1.5±0.2	33.5±4.7	28
169.5	100.4	2.0	0.11	11	-	1.5±0.2	35.0±4.9	35
295.3	151.1	1.5	0.15	10	9±1	3.6±0.5	83.2±11.7	104
482.8	224.0	1.0	0.18	7.6	11±1	4.4±0.6	90.0±12.7	147
754.6	319.6	3.0	0.20	2.2	10±1	6.0±0.8	47.0±6.6	102
1130.7	432.5	3.0	0.35	1.1	12±1	6.3±0.9	33.8±4.8	99
1622.4	551.0	3.0	0.50	0.8	8±1	4.6±0.7	10.0±1.4	35
2228.4	660.9	3.0	0.53	0.7	8±1	5.4±0.8	11.5±1.6	36
2934.8	751.9	2.0	0.60	1.5	8±1	5.8±0.8	10.8±1.5	30
3720.9	820.4	1.0	0.70	3.4	10±1	4.0±0.6	8.0±1.1	18
4565.5	868.9	3.0	0.71	5.5	11±1	11.1±1.6	28.9±4.1	52
5500.0	1000.0	1.0	0.71	7.9	8±1	15.0±2.1	40.0±5.7	72

The dissolved ^{234}Th data for the lower 10 levels are assumed to be equal to $2.3\pm0.2\times10^3$ dpm m^{-3}. The uncertainties in the dissolved ^{228}Ra, ^{228}Th, and ^{230}Th are set at ±10%. The uncertainty in the large-particle ^{228}Th is set at ±50%. The large-particle ^{234}Th and ^{230}Th initial estimates are 80% of the small-particle values with a 20% uncertainty. The initial estimates for the small-particle activities differ from the values one would find if they divided the interpolated activities in Figure 2 by the interpolated total small-particle activities in Figure 3. The difference is caused by the initial estimate of the soft biogenic material small-particle concentration. The initial estimates of the small-particle activity differ from the interpolated values by less than 20%, except in the upper 300 m. See Appendix B for a detailed description of how these values were determined.

k_{-1} in Figure 1) is based on the observed increase with depth of dissolved and small-particle thorium activity [*Bacon and Anderson*, 1982]. Aggregation of small particles into large particles (β_2) throughout the water column is required to explain the observed increase in large-particle activity with depth. The fast-settling velocities (ω) of the large particles are inferred from seasonal variations in thorium activity collected by sediment traps [*Bacon et al.*, 1985]. The disaggregation of large particles (β_{-2}) maintains the concentration of small suspended particles through the water column [*Bacon*, 1984]. Further study of thorium cycling has revealed that remineralization of particles (β_{-1}) could release significant amounts of thorium from the particulate phase to the dissolved phase [*Clegg and Whitfield*, 1991]. The fit of predicted thorium profiles with observations is improved when the release of thorium to the dissolved phase due to the destruction of particulate material is included in the model equations [*Clegg and Whitfield*, 1991]. Active biologic uptake of thorium (β_1) appears to be unlikely, as the uptake of many transuranics and trace metals by living and dead phytoplankton are comparable [*Fisher et al.*, 1983, 1984].

The close coupling between the thorium-cycling model described above and particles in the water column implies an analogous particle-cycling model [*Clegg and Whitfield*, 1990; *Murnane et al.*, 1990]. Here we extend the particle model used by previous investigators to include three different particle types: inert detrital material, "hard" biogenic material, and "soft" biogenic material. These particle types follow different paths in the ocean.

Inert detrital material is introduced into the surface layer from the atmosphere or rivers, whereas hard biogenic material represents carbonate, opal, and other mineral material produced by biota throughout the euphotic zone. Once it is formed, hard biogenic material acts exactly as inert detrital material in the model. As this material sinks through the water column it can aggregate into large particles and disaggregate into small particles; below the euphotic zone there is a constant flux through the water column. Soft biogenic material represents the cycling of particulate organic material. Soft biogenic material forms only in the euphotic zone (β_1), it decays throughout the water column (β_{-1}), and it undergoes exchange between the large- and small-particle classes (β_2 and β_{-2}). This material is produced at a rate $N\beta_1/R^s$ in the euphotic zone where N is a nutrient concentration, β_1 is the particle formation rate constant (which has a nonzero value only in the euphotic zone), and R^s is a Redfield-like ratio that gives the number of moles of type N nutrient per gram of soft biogenic material. R^s is based on soft biogenic material with a phosphorous:nitrogen:carbon ratio of 1:16:130 (see Appendix B for a more detailed discussion). Our treatment of particle decomposition differs from that of *Clegg and Whitfield* [1990] in that the effect of β_{-1} in this model is limited to soft biogenic material in the small-particle phase, whereas remineralization in *Clegg and Whitfield*'s [1990] model affects all of the material in the small- and large-particle phases.

Preliminary modeling results demonstrated the need for three particle types. When β_{-1} operated on only one particle class, particle concentrations dropped to unrealistically low levels below 1 km. Unrealistically high aeolian fluxes were needed if particles were divided into material that was destroyed by remineralization (β_{-1}) and material that was inert detrital material; the same observation was true if the nonremineralized particles were hard biogenic material. Three particle classes produced the most simple, and at the same time realistic, model (i.e., model predictions for most of the water column had reasonable fluxes and concentrations of inert detrital material, hard biogenic material, and soft

biogenic material). We assume that the rates of exchange of thorium between the small- and large-particle phases (β_2 and β_{-2}) also apply to the different particulate phases. This is likely to be an oversimplification, but it is an adequate assumption for these data. This linkage means that both particle and thorium data can be used to determine the rate constants β_{-1}, β_2, and β_{-2}.

Data and Initial Estimates.

Estimates of particle concentrations and fluxes and estimates of thorium isotope activities in solution, on suspended particles, and on material caught by sediment traps, are required if we are to predict the rates of the processes depicted in Figure 1. We have assembled such a data set from several cruises and locations in the northwest Atlantic at and near the Nares Abyssal Plain (23°11'N, 63°58'W [*Cochran et al.*, 1987]; Transient tracers in the Ocean-North Atlantic Study (TTO-NAS) station 24, 23°17'N, 64°09'W [*Key et al.*, 1992]; and Global Ocean Sections Study (GEOSECS) station 31, 27°N, 53°32'W). Appendix B provides a more complete description of the data and a discussion of how the concentrations, fluxes, and activities at different depths were determined. Thorium activities (Figure 2) and particle concentrations and fluxes (Figure 3) at the 13 depths through the water column were based on linear interpolation of data from depths at which samples were collected.

The interpolated thorium activities and fluxes and particle concentrations and fluxes are only part of the information used in finding least squares estimates of the thorium- and particle-cycling rates. We use an inversion technique [*Tarantola and Valette*, 1982] that can incorporate into a solution initial estimates of the value and error for any term, including the unknown rate constants. A more detailed description of how to apply the technique of *Tarantola and Valette* [1982] (hereinafter referred to as TV) to the thorium and particle conservation equations is given by *Murnane* [1993a, 1993b]. The assumptions and methods used to determine the initial estimates for the particle-cycling rates and any unmeasured terms are described in Appendix B. A summary of the thorium and radium activities and their estimated errors that were interpolated from the field data is given in Table 2. Initial estimates and errors for the small- and large-particle concentration of soft biogenic material and the flux of total particulate material at each depth are given in Table 3. Initial estimates for the rates and other constants (ω and R^s) required for the inversion are listed in Tables 4a and 4b. As the inversion is nonlinear, one should be aware that the solutions are dependent on the initial estimates. We discuss the sensitivity of the predicted solutions to different initial estimates in a later section.

A total of 134 equations that describe thorium and soft biogenic particle cycling are used in the inversion. Initial estimates for the 192 measured and estimated terms that are used in the inversion and optimized in a least squares sense include all the thorium analyses (Table 2), the soft biogenic particle concentrations (Table 3), the depth dependent rate constants (Table 4), the dissolved ^{228}Ra activities, ω, and R^s. An advantage of the TV technique is that a solution can be found whether the system is underdetermined or overdetermined. When solving nonlinear systems of equations for either case, the solution must be found by iteration. If the system fails to converge, the solution can be stabilized by altering the covariance matrix (TV). The solution was assumed to have converged when the change in absolute value for every element between consecutive iterative steps was less than 1% of its value from the previous iterative step. An estimated

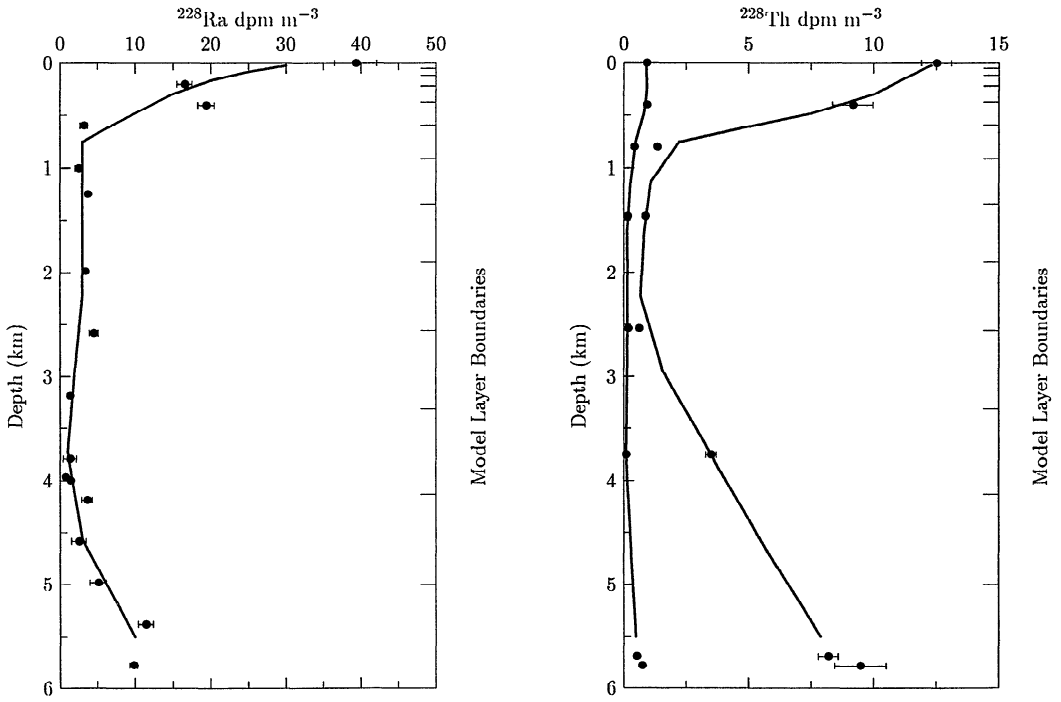

Figure 2. Dissolved ^{228}Ra and dissolved and small-particle ^{228}Th and ^{230}Th profiles. The greater activities at each depth for the ^{230}Th and ^{228}Th are for the dissolved phase. Solid circles for ^{228}Th and ^{230}Th represent the data from *Cochran et al.* [1987], solid circles for ^{228}Ra are from TTO station 24. The horizontal bars show the error estimates for the measurements. The horizontal ticks on the right scale of each figure denote the boundaries between the different levels of the model. The solid lines denote the interpolated activities of thorium and radium through the water column that were used as initial estimates (Appendix B) for the inversion.

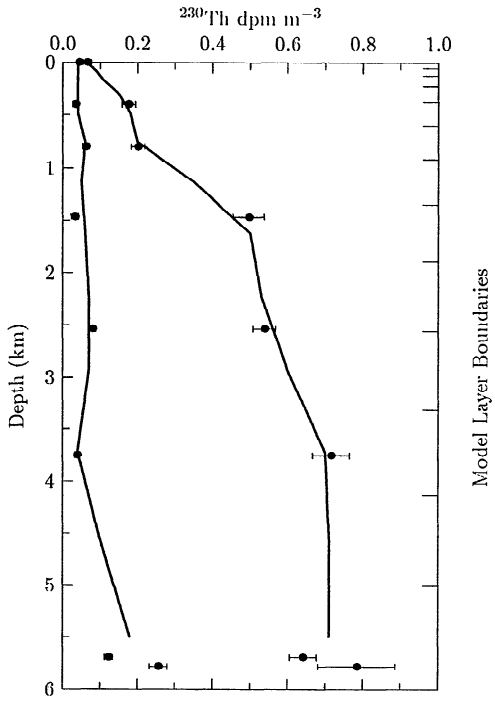

Fig. 2. (continued)

variance for each term can also be determined (TV). The decrease in variance between the initial estimates and the solution provides a measure of how the collected data improve our knowledge (the initial estimates) of the individual terms (TV). The greater the decrease in variance, the more the data constrain the solution and decrease the uncertainty for the given parameter. If the data do not provide any constraints on the initial estimate of a term, then the value and variance for that term will be unchanged.

Lognormal Distributions

For many terms in the model, specifically particle concentrations and rate constants, negative values are physically nonsensical. The lognormal probability distribution, in addition to being applicable to many natural systems, excludes the possibility of negative values. We therefore assume that the following poorly constrained terms have a lognormal probability distribution: the rate constants, settling velocity, R^s, and soft biogenic particle concentrations. This assumption guarantees that physically reasonable values and errors will be found for all terms. Normal and lognormal probability distributions are very similar for terms that are relatively well known if the absolute value of the coefficient of variation (the standard deviation divided by the mean) in the normal distribution is less than 0.2 [*Rothschild and Logothetis*, 1986]. Therefore, for well-constrained parameters, solutions based on a normal or lognormal distribution are likely to be similar. The variances and means for the normal distribution cannot be directly converted to the mean and variance for the lognormal distribution by taking the antilog of the terms (the antilog of the term provides the median). However, as this is a common approach when using lognormal distributions, we will report the results for parameters with lognormal distributions in two ways: (1) as the mean and standard deviation for the lognormal distribution, and (2) as the antilog of the mean of normal distribution, that is, the median of the lognormal distribution.

The least squares solution of the natural log of the variables with lognormal distributions was found by the inversion. The conservation equations were changed slightly to accommodate these terms (Appendix A). For example, β_2 is assumed to have a lognormal probability distribution. The term $exp(\ln(\beta_2))$ was used in the conservation equations, and the least squares estimate of $\ln(\beta_2)$ was found with the inversion.

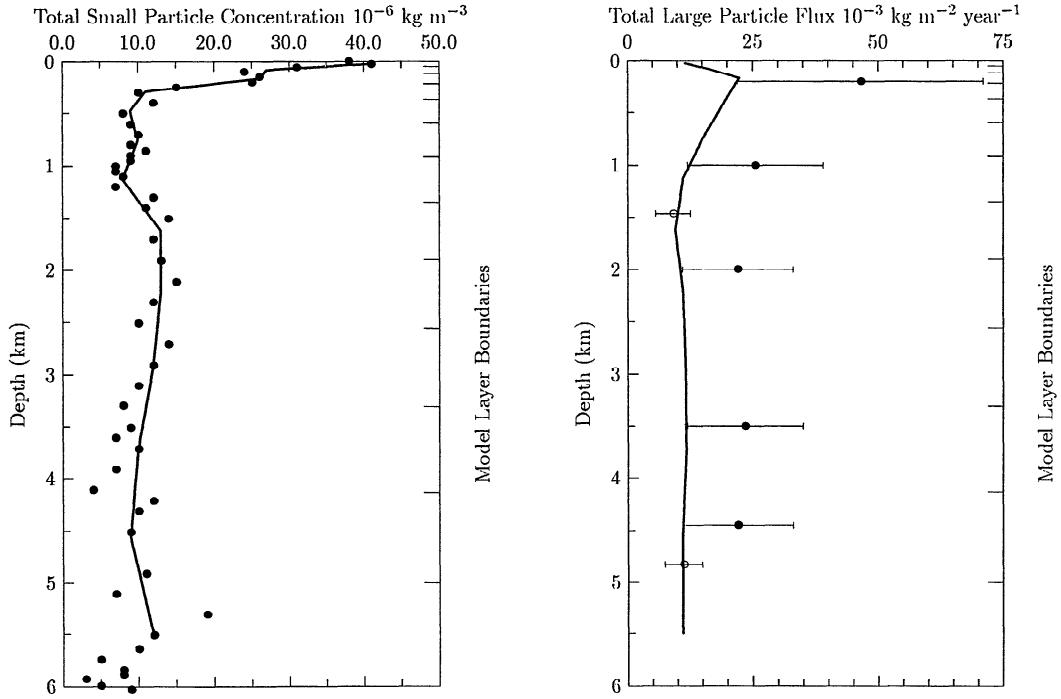

Figure 3. Suspended particle concentrations and flux measurements at Nares. The concentration measurements are from GEOSECS station 31. The flux data at 1464 m and 4832 m (open circles) are from *Fisher et al.* [1988], the remaining flux data are from *Hargrave* [1985]. The solid circles give actual measurements, and the horizontal bars are one standard deviation. The horizontal ticks on the right scale and solid lines are as in Figure 2.

Table 3. Initial Estimates of Particle Terms for Inversion

Depth, m	P_S^s, 10^{-6} kg m^{-3}	P_L^s, 10^{-6} kg m^{-3}	F_{P_L}, 10^{-3} kg m^{-2} y^{-1}
25.5	57±530	0.1±0.2	11.6
85.1	18±190	0.2±0.3	16.4
169.5	27±260	0.2±0.4	22.4
295.3	8±100	0.2±0.3	20.8
482.8	6±70	0.2±0.3	18.5
754.6	2±39	0.1±0.2	15.1
1130.7	2±22	0.04±0.19	11.2
1622.4	2±16	0.02±0.18	9.6
2228.4	3±32	0.04±0.20	11.2
2934.8	3±31	0.05±0.20	11.6
3720.9	3±31	0.06±0.20	11.8
4565.5	2±22	0.04±0.19	11.0
5500.0	2±24	0.04±0.19	11.0

Soft biogenic material concentrations are used as initial estimates for the inversion. The relatively large uncertainties for the particle concentrations are based on error propagation. The flux data were assigned an uncertainty of ±50%. The initial concentrations of inert abiogenic particles and hard biogenic particles are $P_L^i = 4.9\pm6.5\times10^{-8}$ kg m^{-3}, and $P_L^h = 1.1\pm0.8\times10^{-7}$ kg m^{-3} (for layer 3 and below). P_L^h linearly decreases to zero at the surface. Using these P_L^h and P_L^i concentrations, P_S^h and P_S^i were found using the relationship $P_S^* = P_L^*\beta_{-2}/\beta_2$ (where the asterisk is either h or i) and the rates given in Table 4. For the top two layers, the relationship for P_S^h is $P_S^h = (P_L^h\beta_{-2} + \omega\partial P_S^h/\partial z)/\beta_2$. See Appendix B for a more complete discussion of how these values were found.

Inversion of Nares Data

Results

The difference between the initial estimate of a term and its value predicted with the inversion is a function of the initial uncertainty associated with the term (its standard deviation). For a given set of data the value of a term can change over a larger range as its initial uncertainty increases. Because of this we present the results weighted by the initial uncertainty for each term: $(x_\circ - x)/\sigma_\circ$, where $x_\circ$ is the initial estimate for a term, $\sigma_\circ$ is the initial estimate of the term's standard deviation, and x is the value of the term predicted with the inversion. The weighted change between the initial estimate and predicted value for most of the T( ) terms is greater than the weighted change between the initial estimate and predicted values for the rates and measured activities (Figure 4a). None of the predicted values for T( ) exactly equal zero. The values of the rate constants predicted with the inversion change by the greatest weighted amounts among the terms in SMS( ) for the particle and thorium conservation equations. The predicted values for the rates are within previous estimates for the rate constants (Table 1) and differ from their initial estimates (Table 4) by less than 30%.

An examination of the covariance matrices predicted with the inversion can also provide information on how the data set increases our knowledge of the terms optimized in a least squares sense. We weight the difference between the initial estimate and the predicted value of the standard deviation by the standard deviation of the initial estimate $((\sigma_\circ - \sigma)/\sigma_\circ$, where $\sigma_\circ$ is the initial estimate of the standard deviation of a term and σ is the standard deviation predicted with the inversion) to examine the decrease in variance for all the terms predicted with the inversion. The greatest weighted change in the standard deviation occurs for the T( ) terms (Figure 4b). The terms in SMS( ) with the greatest decrease in standard deviations are the rate constants (except for β_1) and the dissolved ^{234}Th terms. Standard deviations for the rate constants remain large. Predicted standard deviations for the measured terms ^{230}Th and ^{228}Th differ little, if at all, from the initial standard deviations. The inversion has improved our knowledge of T( ) and the rate constants, but it has done little to constrain further the interpolated activities for the thorium isotopes.

The sensitivity of the inverse solution to different initial guesses for the rate constants and R^s was tested because the solution is dependent on the initial estimates of the values and uncertainties. The sensitivity tests involved doubling and halving the initial estimates of the rate constants and R^s. Among the unaltered terms, T( ) displayed the largest differences between the results from the sensitivity tests and the results from the original solution. The relative change between the initial estimates and predicted values for terms that were altered in the sensitivity tests was similar to the original solution except for the rate constant k_1. For example, when the initial estimate of k_1 was doubled to 10.0×10^4, its solution changed to 8.8×10^4 (values for k_1 are the natural log of the initial value with units of cubic meters per kilogram per year). This can be compared to the original initial estimate, 5.0×10^4, and the inverse solution, 4.9×10^4. When initial values of β_{-2} were doubled or when the initial values of β_2 were halved the inversion would not converge. This occurs when the terms optimized in a least squares sense do not both satisfy the conservation equations and allow the cost function to be at a minimum.

Discussion

The rate constants predicted with the inversion technique (Table 4) are within the range of previous estimates (Table 1). Except for k_1 and k_{-1} the rate constants are poorly constrained by the data. Possibly the most interesting features of the results are the relatively constant values of β_2 and β_{-2} through the water column. Previous estimates of these rate constants as a function of depth [*Clegg et al.*, 1991; *Clegg and Whitfield*, 1991] suggested that the rates varied by 1 order of magnitude to several orders of magnitude through the water column. This wide range in rate constants is not needed to satisfy the constraints imposed by the Nares Abyssal Plain data set compilation.

Although the rates predicted with the TV technique do not vary greatly through the water column, it seems reasonable to expect changes in aggregation and disaggregation of particles with depth. Large variations in aggregation and disaggregation rate constants, however, have yet to be rigorously documented and the values that are published (Table 1) may be biased by a priori assumptions. For example, the large range in rate constant values for particle and thorium cycling predicted by *Clegg and Whitfield* [1990, 1991] are partially the result of assumptions in their model. *Clegg and Whitfield* [1990] specify particle concentration and particle flux profiles through the water column, assume that below 1 km, $r_{-1} = 148$ y^{-1} (where r_{-1} is equivalent to β_{-2} and 148 y^{-1} is the lower limit of values from *Nozaki et al.*, [1987]), and calculate r_1 (equivalent to β_2) using the equation

$$r_1 = (P_L r_{-1} + P_r - P_s\gamma)/P_s$$

Here, γ is the particle remineralization rate, P_s is the suspended particle concentration, P_r is the production rate of particles (which is zero below 100 m), and P_L is the sinking particle concentration.

Table 4a. Initial Estimates and Predicted Values for Rate Constants

	$\beta_{-1}y^{-1}$			$\beta_2 y^{-1}$		$\beta_{-2}y^{-1}$	
Depth m	Initial Estimate	Predicted Median	Predicted Mean	Predicted Median	Predicted Mean	Predicted Median	Predicted Mean
25.5	35±19	31 (9 - 113)	70±137	2.8 (0.6 - 12.6)	9±24	156 (14 - 1760)	2690 ± 10^4
85.1	88±31	74 (8 - 673)	798±7940	3.6 (0.8 - 16.1)	11±30	147 (14 - 1580)	2280 ± 10^4
169.5	45±21	37 (4 - 328)	378±3520	3.2 (0.6 - 17.4)	13±50	149 (15 - 1460)	1880 ± 10^4
295.3	1.3±8.7	1.2 (0.3 - 61)	1766 ± 10^7	3.2 (0.5 - 20.8)	18±89	140 (19 - 1010)	950±5700
482.8	1.8±9.1	1.4 (0.7 - 29)	113 ± 10^4	3.2 (0.5 - 20.0)	17±77	136 (19 - 960)	870±5000
754.6	4.4±11.9	3.8 (0.1 - 116)	1010 ± 10^6	3.1 (0.5 - 19.2)	16±73	149 (28 - 790)	580±2000
1130.7	2.4±4.9	2.3 (0.2 - 25)	36±560	2.3 (0.4 - 13.3)	11±43	160 (28 - 900)	700±2700
1622.4	1.4±3.8	1.5 (0.1 - 16)	24±371	3.2 (0.7 - 14.0)	9±25	148 (20 - 1080)	1020±6300
2228.4	1.0±3.1	1.0 (0.9 - 11)	16±250	2.9 (0.6 - 13.5)	9±28	143 (21 - 970)	860±4600
2934.8	0.7±2.7	0.7 (0.7 - 8.0)	12±193	2.5 (0.5 - 12.6)	9±30	163 (27 - 1000)	820±3700
3720.9	0.6±2.4	0.6 (0.5 - 6.6)	10±162	2.5 (0.5 - 12.4)	9±28	158 (27 - 920)	720±2900
4565.5	0.5±8.0	0.5 (0.0 - 53)	$10^4\pm10^{10}$	3.0 (0.6 - 14.1)	10±28	146 (22 - 940)	810±4000
5500.0	0.2±1.5	0.2 (0.2 - 2.6)	4±64	2.1 (0.4 - 10.7)	8±27	196 (33 - 1150)	920±3800

The initial estimate throughout the water column was $3.0\pm27\ y^{-1}$ for β_2 and $155\pm1610\ y^{-1}$ for β_{-2}. The standard deviation for the initial estimates were found by error propagation (appendix B). The predicted median values are the antilog of the normal solution. The values in parentheses are the antilog of the sum of the mean, minus and plus, one standard deviation from the normal solution. The predicted means are the minimum variance unbiased estimates of the mean and standard deviation of the lognormal distribution (assuming the calculated covariance matrix approximates the true covariance).

Above 1000 m, r_{-1} was set proportional to γ. The assumptions about the behavior of r_{-1} and γ through the water column forces r_1 to change in a predetermined manner. Most other estimates of β_2 and β_{-2} determined from field data offer little additional information on the change in rates with depth and represent depth-averaged values from individual localities [*Nozaki et al.*, 1987; *Murnane et al.*, 1990; *Lavelle et al.*, 1991].

For the inversion we attempted to minimize assumptions about the changes in β_2 and β_{-2} as a function of depth by using constant initial estimates with large variances for β_2 and β_{-2}. The predicted rates change by less than 30% from the initial estimates, and the predicted standard deviations do not decrease greatly from the estimated initial variances (Table 4). The inversion results suggest that β_2 and β_{-2} at the Nares Abyssal Plain are not strongly constrained by this compilation of data, by the initial estimates of unmeasured terms, or by the errors associated with all the terms. Without additional data it seems difficult to justify any functionality beyond first-order kinetics for the aggregation and disaggregation of particles at the Nares Abyssal Plain. Despite the small (and statistically insignificant) change in the rate constants for aggregation and disaggregation through the water column, we can partially satisfy our intuition concerning particle aggregation and disaggregation by noting that there is still a large change in the flux of particles and thorium between the particle classes as particle concentrations and activities change.

A stronger case can be made for the variation of β_{-1} through the water column because of its association with remineralization and the strong decrease in the flux and concentration of soft biogenic material with depth. Initial estimates for β_{-1} were based on the conservation equation for soft biogenic material (see Appendix B for details) and decreased by 2 orders of magnitude through the water column. If $T(P_S^s) = 0$, then the equation for soft biogenic material in the small-particle phase below the euphotic zone can be used to find that

$$\beta_{-1} = \frac{\beta_{-2} P_L^s}{P_S^s} - \beta_2$$

This approach includes assumptions about the behavior of particle fluxes, assumptions about the relative percentage of soft biogenic material in particles, and assumptions associated with linearly interpolated small-particle concentrations. These assumptions appear to be consistent with the information contained in all of the data because the median values for β_{-1} predicted with the inversion technique change by less than 20% from the initial estimates. However, the estimated uncertainties of the predicted β_{-1} are still relatively large and suggest that there is no statistically significant difference between the values of β_{-1} at different depths.

Four other terms related to particle cycling (β_1 in the top two layers, R^s, and ω) have predicted values that are essentially unchanged from the initial estimates. The data do not constrain these terms beyond our prior estimates of their value (Table 4b, Appendix B).

Given the large uncertainties in the rate constants and the probable importance of T( ) in the water column (see below), it does not appear necessary to assume that k_1 changes through the euphotic zone as suggested by *Clegg and Whitfield* (1991). The Nares thorium data can easily be satisfied through deviations from one-dimensional steady state conditions.

The measured activities and concentrations optimized with the TV inversion technique are usually assumed to be known exactly or are not considered when calculating thorium and particle-cycling rate constants by other methods. The predicted values do

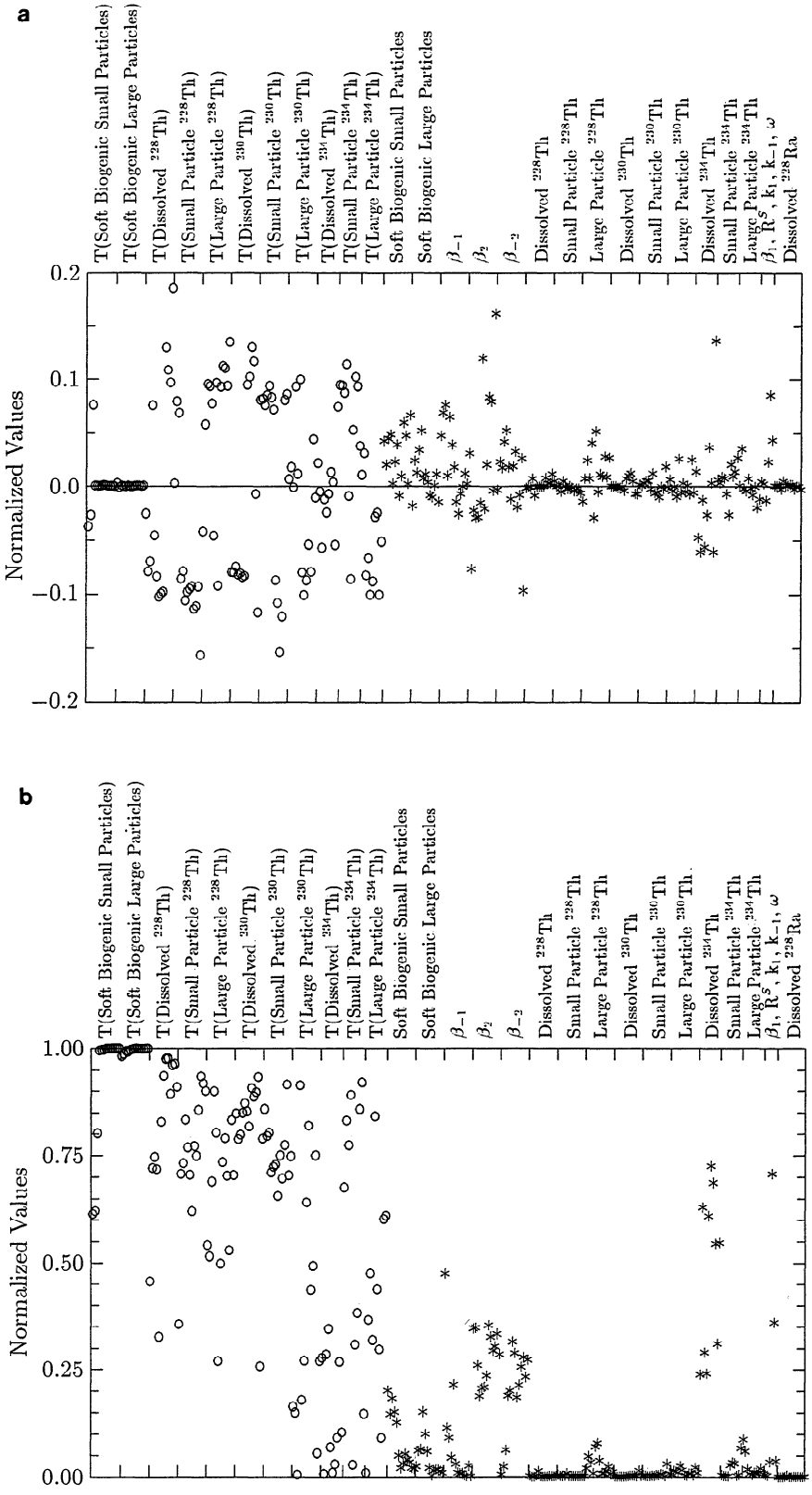

Figure 4. Plots of weighted inversion results. For each term the results are ordered from the surface layer value on the left to the bottom layer value on the right. (a) Plot of weighted residuals; $(\hat{x}^i - x^i)/\sigma^i_\circ$ for each unknown in the inversion, where $x^i_\circ$ and $\sigma^i_\circ$ are the initial estimates of the value and standard deviation for each term and x^i is the value predicted with the inversion. The open circles denote the weighted T( ) found with the inversion. The asterisks denote the weighted terms in SMS( ) predicted with the inversion. (b) Plot of weighted change in standard deviation; $(\hat{\sigma}^i_\circ - \sigma^i)/\sigma^i_\circ$ for each term. The symbols and their order match Figure 4a. The predicted standard deviations are not rigorous estimates because of the nonlinear equations.

Table 4b. Initial estimates and predicted values for remaining parameters

Parameter	Initial Estimate	Predicted Median	Predicted Mean
$\beta_1(1)$, y^{-1}	16.8±11.9	17 (9.8 - 28.5)	19±11
$\beta_1(2)$, y^{-1}	10.7±7.6	11 (6.3 - 18.2)	12±7.0
k_1, $10^4\ m^{-3}\ kg^{-1}\ y^{-1}$	5.0±5.0	4.9 (4.0 - 6.0)	5.0±1.0
k_{-1}, y^{-1}	3.0±3.0	2.8 (1.8 - 4.4)	3.1±1.5
R^s, 10^{-4} mol g^{-1}	2.34±4.68	2.38 (0.82 - 6.86)	4.14±5.82
ω, m d^{-1}	150±100	147 (90 - 238)	165±84

The standard deviation for the initial estimates were found by error propagation (appendix B). The predicted median values are the antilog of the normal solution. The values in parentheses are the antilog of the sum of the mean minus and plus one standard deviation from the normal solution. The predicted means are the minimum variance unbiased estimates of the mean and standard deviation of the lognormal distribution (assuming the calculated covariance matrix approximates the true covariance).

not differ significantly from their initial estimates because of the relatively small uncertainties of the initial estimates (usually ±10%).

The predicted values of the T( ) terms differ from their initial estimates by a relatively large amount (Figure 4a). The initial estimates for T( ) were all equal to zero with a large uncertainty based on the value of the initial estimate of SMS( ) (see Appendix B). Setting T( ) = 0 is equivalent to assuming that the sum of the conservation equation time dependence and transport terms are negligible. The large uncertainty for T( ) permits the predicted sum to differ greatly from zero. The large error also can be viewed as including model errors in the inverse solution [*Menke*, 1984]. Small initial uncertainties for T( ), which would force the solution closer to one-dimensional steady state conditions, do not allow the inversion routine to converge. This implies that the conditions at the Nares Abyssal Plain are inconsistent with one-dimensional steady state assumptions about thorium and particle cycling.

The assumption that T( ) equals zero, or is negligible, can be tested by comparing the predicted magnitudes of each process included in SMS( ) with the predicted value of T( ). If the assumption that T( ) is negligible or zero is correct, then the predicted T( ) for each phase should be much smaller than the other terms in the conservation equation for a given phase. Thorium activities, particle concentrations, and rate constants predicted with the inversion are used in this comparison. A comparison of T( ) to the terms in SMS( ) reveals that in general T( ) is not small relative to other processes affecting a given particle or thorium phase (Table 5). For example, depth profiles of small-particle and dissolved thorium fluxes produced by various interactions (Figure 5) show that T( ) can be important throughout the water column. There remains the possibility that T( ) = 0 may be true for each data set and that terms in SMS( ) at the time each data set was collected are incompatible.

The magnitude of T( ) for each phase is not unreasonable. For example, T( ) at 3800 m is the second largest term affecting dissolved ^{230}Th (≈ 0.25 disintegrations per minute (dpm) $m^{-3}\ y^{-1}$, Figure 5). Assuming that transport is negligible and that T( ) is dominated by the time rate of change term one can infer that thorium activity at this depth would change by ≈ 0.1 dpm m^{-3} over a 6-month period. This is nearly 15% of the measured ^{230}Th activity for this depth and not much greater than the analytical precision for the dissolved thorium analysis. If T( ) was due to advective processes only and there was a relatively slow horizontal velocity of 0.01 m s^{-1}, then ^{230}Th activity would need to change by only 10^{-2} dpm m^{-3} over 10 km. Changes in dissolved ^{230}Th activity of this order are not difficult to imagine. If the true value of T( ) is close to the T( ) predicted with the inversion, then one should not neglect T( ) (i.e., set T( ) = 0) when calculating particle- and thorium-cycling rate constants.

Table 5. Comparison of Major Processes Affecting Thorium and Particle Phases

	Dominant Processes		
	Dissolved Phase	Small-Particle Phase	Large-Particle Phase
Soft biogenic particles		production*, β_{-1}*, aggregation, disaggregation	T( ), aggregation, disaggregation, settling*
^{234}Th	production, decay	decay, adsorption	aggregation, disaggregation
^{230}Th	T( ), β_{-1}*, adsorption†, desorption†	adsorption, desorption, aggregation, disaggregation, T( )	aggregation, dissagregation, settling*
^{228}Th	T( ), adsorption, β_{-1}*, decay, production	T( ), adsorption, β_{-1}*, disaggregation	aggregation, disaggregation, settling*, T( )*

* Upper water column
† Lower water column

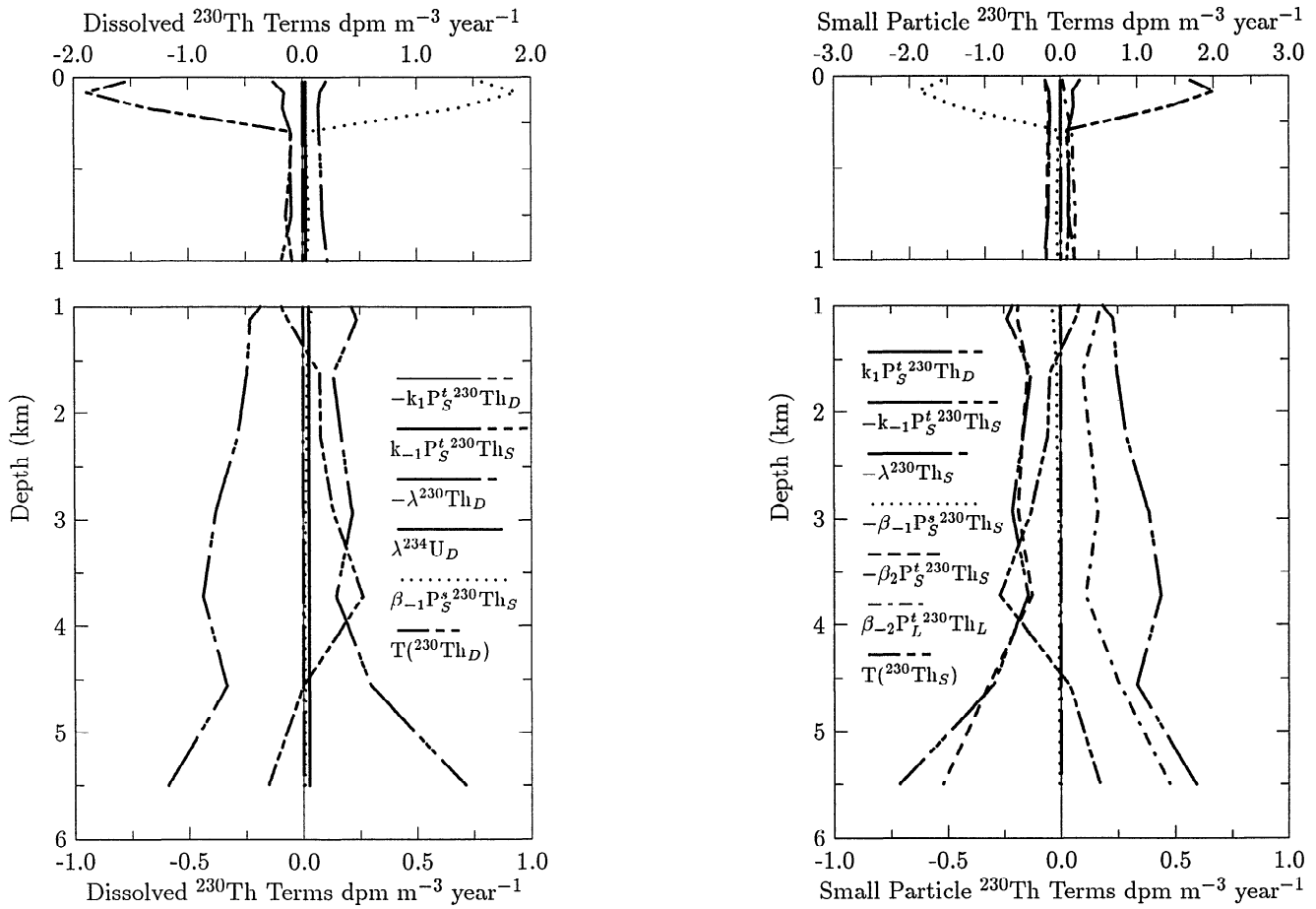

Figure 5. Depth versus the change in ^{230}Th activity with time (disintegrations per minute per cubic meter per year) caused by different terms in the conservation equations for the dissolved, small-, and large-particle phases. T( ) and the rates and activities used to calculate the terms are from the inversion results. Note the change in scale for both axes.

The dominant term in the predicted values of T( ) could be either transport or time dependence. One way of determining this is to determine if T( ) changes at water mass boundaries. Changes near water mass boundaries would suggest that transport along isopycnal surfaces could be important. At TTO-NAS station 24, there are inflections in the slope of sigma 4 versus depth at 200, 400, ≈1200-1400, and ≈3900 m; the most defined change in slope occurs between 1200 and 1400 m. The inflections are roughly located where there is a large increase of small-particle concentrations with depth (Figure 3). The correlation between the shift in particle concentration and water mass boundary is circumstantial evidence that lateral transport may be significant for the distribution of small particles. A sharp change in the ratio of β_2/β_{-2} could also change the small-particle concentration but would be inconsistent with a reasonable assumption of smoothness in the profiles of the rate constants as a function of depth. Neither ^{230}Th nor ^{228}Th data show a correlation with changes in water mass boundaries (Figure 2).

Time dependence could be the dominant term in T( ) for other conservation equations. The mean activity flux for ^{230}Th found by both sediment traps is slightly lower than the theoretical flux needed for complete removal of ^{230}Th from the water column overlying the sediment traps. This implies that time dependent processes may be important in the flux of large particles, that lateral transport affects the ^{230}Th budget, or that the sediment trap may not be 100% efficient at collecting material. Variations in thorium and mass fluxes over time are known to occur [*Bacon et al.*, 1985; *Deuser*, 1986], so time dependent processes could also be an important contributor to T( ) for large-particle phases. Other workers find that up to 1/3 of the ^{230}Th produced in the overlying water column can be removed by lateral transport [*Anderson et al.*, 1983; *Bacon et al.*, 1985]. Lateral transport of large particles would seem unlikely to be a significant factor if these particles have settling velocities on the order of 150 m d^{-1}. However, work by *Deuser et al.* [1990] shows that the best correlation between surface production as determined by satellite data, and deep particle flux, occurs with surface source areas that are not directly above the sediment trap. *Siegel et al.* [1990] also discuss the importance of Lagrangian effects on sediment trap data. Finally, thorium fluxes based on sediment trap measurements and thorium budgets do not always agree [*Buesseler*, 1991]. These observations suggest that one may have to consider time dependence and lateral transport when working with material in the dissolved, small-particle, and large-particle phases.

One implication of this discussion is that the wide range of values for β_2 and β_{-2} listed in Table 1 may not actually be caused by processes that occur in the water column. Instead, the variation could reflect assumptions made in estimating the rate constants (e.g., one-dimensional steady state conditions and/or data averaging). The initial estimates of these parameters at the Nares

Abyssal Plain provide an example. In Appendix B we note that the data from level 11 were neglected when the depth-averaged values of the small-particle ^{230}Th activity were found. If the low activity at this depth was included, the initial estimate for β_{-2} would change from $\beta_{-2} = 155\ y^{-1}$ to $\beta_{-2} = -336\ y^{-1}$, a physically unrealistic value. The sensitivity of the rate constants to small changes in the averaged data is a result of the ^{230}Th and particle conservation equations nearly being colinear. As a result, small changes in the data can have dramatic effects on calculations to determine β_2 and β_{-2}. If the data used to calculate the rate constants in Table 1 are nearly colinear or if T( ) is significant but not included in the calculations, then the values of the predicted rate constants could be significantly in error.

The sensitivity tests reveal several features of the inversion solution. The first is that changing the initial estimates by a factor of 2 for a given set of rate constants barely alters the predicted value of the unaltered terms in SMS( ). This is because the large initial variance associated with T( ) allows changes in the predicted T( ) to dampen the effects of the altered parameter. The second is that the particle-cycling rate constants β_2 and β_{-2} are coupled to changes in k_1 and k_{-1}. Changing k_1 or k_{-1} affects the thorium activity, which changes the best fit β's, which in turn alters the particle distributions. The third point is that k_1 is the only rate that is well constrained by the data; this is consistent with its relatively small estimated standard deviation (Table 4). The value of k_{-1} is not as well constrained, possibly because the effects of other processes, such as the release of thorium to the dissolved phase through the action of the rate constant β_{-1}, are important. These results differ from the observations of *Lavelle et al.* [1991] who found that k_1 and k_{-1} were linear functions of each other.

Several observations summarize the results of the inversion. The large predicted errors suggest that the rates are poorly constrained by the data and that little variation in particle aggregation and disaggregation rate constants is needed for the conservation equations to be consistent with the data. The nonzero values for T( ) suggest that time dependence, advective, and/or diffusive transport are important. The sensitivity tests show that although the predicted rates are a function of the initial estimates, the general pattern of relative constant aggregation and disaggregation rates through the water column is unchanged.

We now use the rates predicted with the inversion in a one-dimensional steady state forward model of particle and thorium cycling. The thorium and particle profiles predicted with the forward model support the conclusions based on the inverse results and suggest additional measurements that would better constrain the rate estimates.

Forward Model

The forward model uses the conservation equations for the thorium isotopes and soft biogenic material in each phase and the assumption that T( ) equals zero. The concentrations of inert detrital and hard organic material in the large-particle phase are fixed as in the inversion. The concentrations of inert detrital and hard organic material in the small-particle phase are based on the predicted values of β_2 and β_{-2} at each level. The sensitivity of the forward model profiles to changes in the rate constants is useful in understanding the precision with which thorium and particle data must be known in order to precisely determine different rate constants. The forward model sensitivity tests we present use the rates predicted by the inversion sensitivity tests when the initial estimates of the rates β_2, k_1, k_{-1}, and both β_{-2} and β_2 were doubled throughout the water column. In the following discussion we will refer to the forward profiles predicted using the rates in Table 4 as the "standard case".

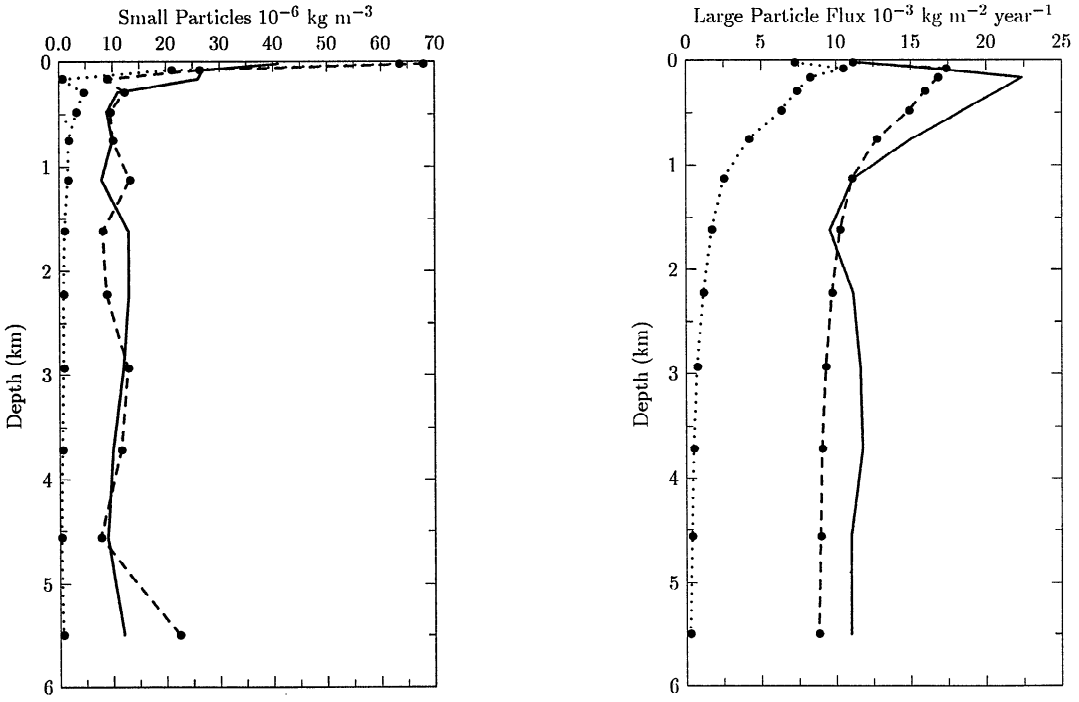

Figure 6. Forward model predictions of small-particle concentrations and large-particle fluxes using rate constants from the inversion. The solid lines represent the interpolated concentrations and fluxes for the total particulate material that were shown in Figure 3. The solid circles denote the calculated values at each depth in the model. The dotted line gives the soft biogenic material data and the dashed line the total of the soft biogenic, hard biogenic, and inert detrital material.

Results

The total small-particle concentrations and fluxes predicted with the forward model are reasonable approximations of the interpolated data except for the low particle concentrations and fluxes of soft biogenic material in the deeper parts of the water column (Figure 6). The total particle flux data agree, within sampling error, with the sediment trap observations at the two sampled depths, but the calculated flux of organic carbon (0.05 mol C m^{-2} y^{-1} at 1.6 km and 0.01 mol C m^{-2} y^{-1} at 4.5 km; based on the predicted R^s and a C/P ratio of 130) is lower at the deeper depth than the value reported by *Fisher et al.* [1988] (0.04±0.02 mol C m^{-2} y^{-1} at both 1.5 km and 4.8 km). Dissolved and small-particle ^{228}Th and ^{230}Th activities predicted by the forward model differ from the interpolated data through most of the water column (Figure 7). Within the measurement error, however, the ^{230}Th activity flux predicted with the forward model (48 dpm m^{-2} y^{-1} at 1.6 km and 127 dpm m^{-2} y^{-1} at 4.6 km) agrees with the sediment trap observations *Fisher et al.* [1988] (33.5±15.9 dpm m^{-2} y^{-1} at 1.5 km and 101±46 dpm m^{-2} y^{-1} at 4.8 km). The ^{228}Th activity fluxes predicted with the forward model (500 dpm m^{-2} y^{-1} at 1.6 km and 290 dpm m^{-2} y^{-1} at 4.6 km) match the 1.5 km sediment trap observation and are lower than the 4.8 km data point *Fisher et al.* [1988] (574±312 dpm m^{-2} y^{-1} at 1.5 km and 588±217 dpm m^{-2} y^{-1} at 4.8 km).

The activity, concentration, and flux profiles predicted with the forward model and rates from the inversion sensitivity tests differ from the standard case in a predictable manner. In all cases the ^{230}Th activity flux is unchanged in the one dimensional model because the activity removed by sinking particles must essentially balance the activity produced by the decay of the dissolved parent nuclide. Doubling β_2 changes both thorium and particle profiles significantly by lowering small-particle activities and concentrations. Doubling k_1 increases small-particle thorium activities, and doubling k_{-1} decreases small-particle thorium activities.

An important result from the sensitivity tests comes from the observation that when both β_2 and β_{-2} are doubled, the forward model profiles for the concentrations and fluxes of thorium and total particles do not change greatly whereas the profiles for soft biogenic matter change dramatically. For example, the profiles predicted during the sensitivity tests show that: (1) the activities of the thorium isotopes in the dissolved and small-particle phases generally differ from the standard case by less than 20% (except near the surface and bottom), (2) the flux of ^{228}Th and ^{234}Th differs greatly from the standard case only near the surface, and (3) the small-particle concentrations of P_S^h and P_S^i change by less than 20% through most of the water column.

Large differences in profiles of soft biogenic matter are predicted when both β_2 and β_{-2} are doubled (Figure 8). The concentration of soft biogenic small particles is 25-50% of the standard case in the euphotic zone, near the standard case between the euphotic zone and 1 km depth, and more than 1 order of magnitude lower than the standard case at depth. The flux of soft biogenic large particles is approximately equal to the standard case at the surface and 1 order of magnitude lower than the standard case at depth. These relatively large changes are in contrast to the smaller changes in profiles for hard biogenic material, inert abiogenic material and thorium isotopes that were described above.

Discussion

The results from the forward model differ slightly from a one-dimensional steady state model that includes advection and diffusion. However, the differences produced by neglecting advection and diffusion in this one-dimensional model seem likely to be on the same order as those introduced by assuming unknown (and possibly incorrect) advection velocities and eddy diffusion coefficients. With this simplification in mind we can still obtain some insights relevant to the determination of particle-cycling rate constants. The largest differences between the interpolated

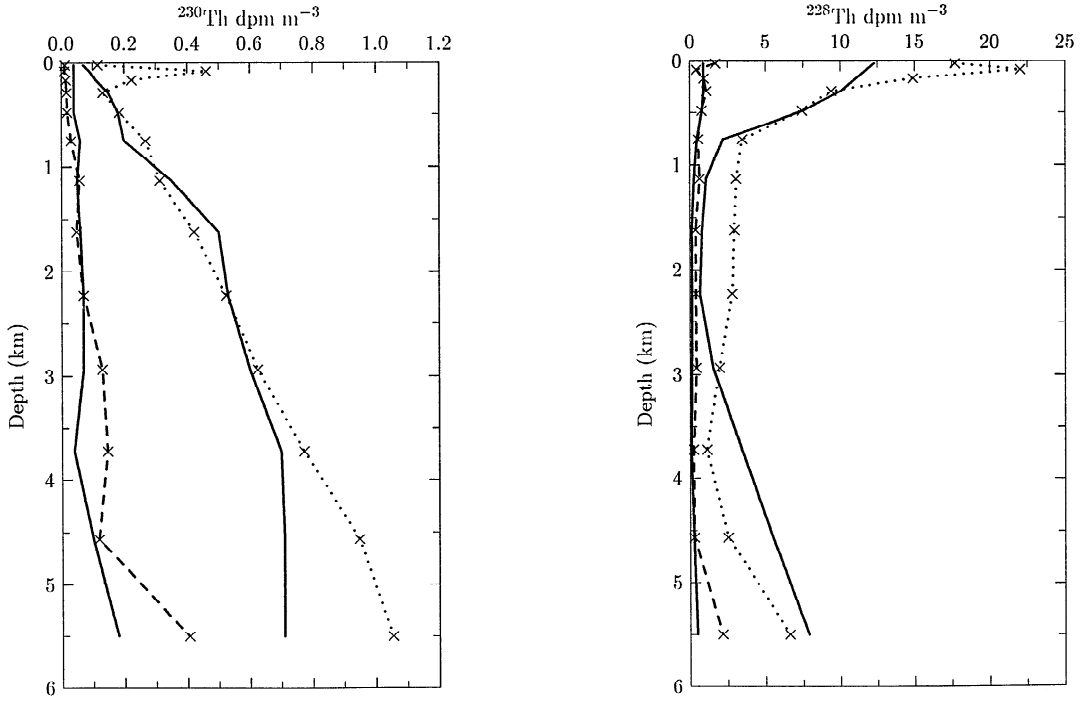

Figure 7. Forward model predictions of ^{230}Th and ^{228}Th dissolved and small-particle activities. The solid lines represent the interpolated activities that were shown in Figure 2. The higher activities are for the dissolved phase. The x denote the calculated activities at each level; the dotted lines give the dissolved activities, and the dashed lines give the small-particle activities.

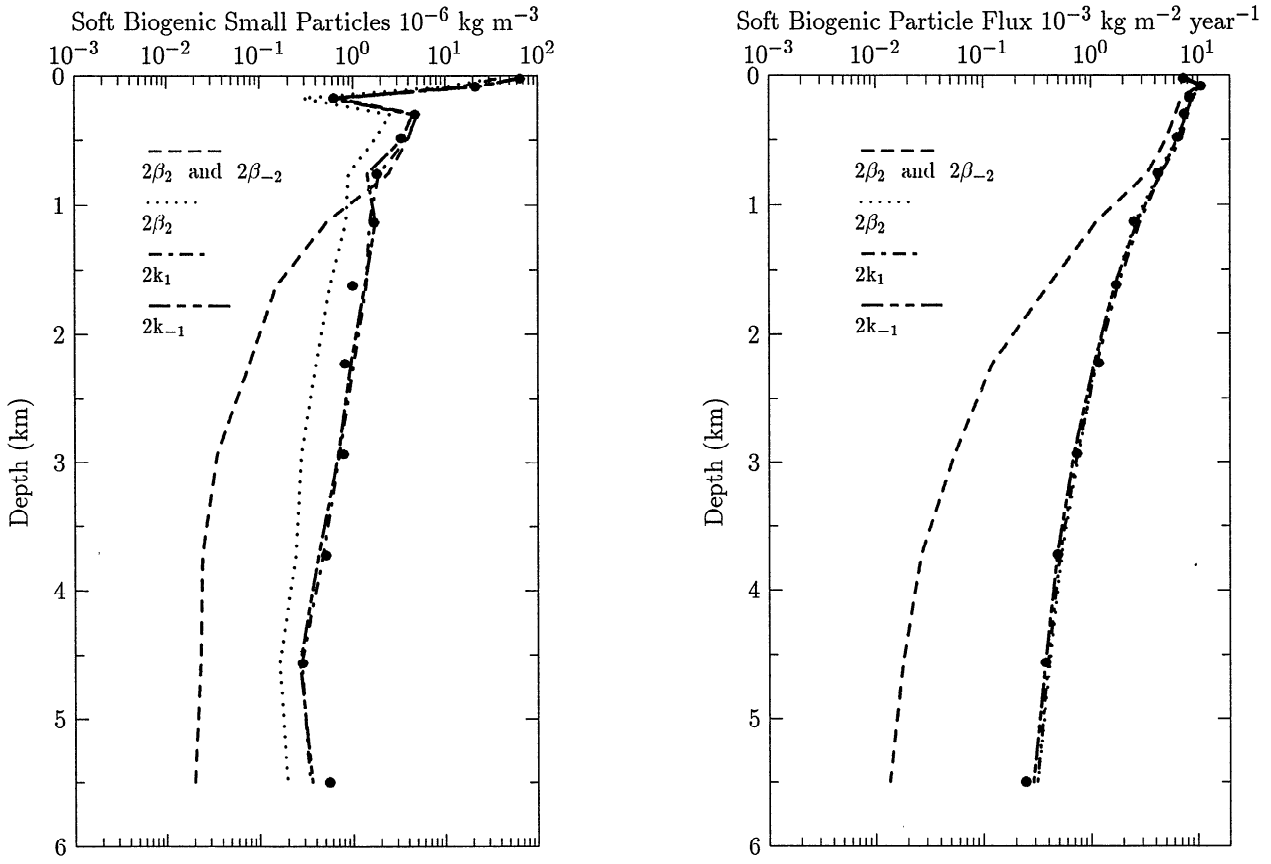

Figure 8. Forward model profiles of soft biogenic material small-particle concentrations and large-particle fluxes predicted with rate constants from the inversion sensitivity tests. The results from the standard case (Figure 6) are given by the solid circles. The legend shows how the initial estimates of the rates differed from the standard case. Note the logarithmic concentration scale.

profiles and the forward model results for ^{230}Th (except dissolved ^{230}Th at depth) and ^{228}Th tend to occur where the values of T( ) are large (compare Figures 5 and 7). These differences suggest that T( ) has a major role in the development of the measured particle and thorium profiles for the northwest Atlantic Ocean.

The good match between predicted and observed ^{230}Th profiles that *Clegg et al.* [1991] obtain for the station P data from the North Pacific can be attributed to the almost monotonic increase in ^{230}Th with depth at that locality, which is consistent with a small value for T( ). As a result, neglecting T( ) while estimating the rate constants with ^{230}Th data may be a good assumption in the North Pacific. The fit between their predicted and observed ^{228}Th profiles, however, is not as good as that for ^{230}Th. They improve the predicted ^{228}Th profile by changing the measured ^{228}Ra source for the middepths of the water column. An interpretation of the data consistent with our approach would be that the radium data are correct and that the poor fit is a result of unaccounted terms such as time dependence and lateral transport.

The different profiles produced by the forward model using rate constants from the sensitivity tests illustrate the precision with which the data must be measured in order to uniquely determine the particle-cycling rate constants. If the profiles differ from the standard case by more than 10%, roughly the analytical precision of a measurement, then an inversion of data from the profiles should yield distinctly different estimates for the rate constants. The forward model thorium profiles clearly differ from the standard case when changes are made in k_1, k_{-1}, or β_2. As a result, estimates of k_1 or k_{-1}, which are not directly related to the cycle of particles (or organic carbon) in the ocean, can be made using the thorium data. Thorium as well as total particle profiles differ greatly from the standard case when β_2 is doubled and shows that the ratio of β_2/β_{-2} can be estimated easily from the total particle profiles or the thorium data, as previously noted by *Clegg and Whitfield* [1990, 1991]. If the ratio of β_2/β_{-2} remains constant, then changes in β_2 and β_{-2} significantly affect modeled thorium activities or total particle concentrations in regions with large changes in mass and activity gradients. Unfortunately, these regions, such as the surface ocean, are where T( ) is likely to be relatively large. These results suggest that only the ratio of β_2/β_2 can be precisely determined from an inversion of total particle and thorium profiles.

Soft biogenic material is the only phase in our model that is sensitive to the value of β_2 and β_{-2} when the ratio of β_2/β_{-2} is constant (Figure 8). The profiles predicted using rates from the inversion sensitivity tests imply that more precise estimates of β_2 and β_{-2} could be made if the errors in the estimated concentrations of soft biogenic material (Table 3) were smaller. Similarly, if we equate particulate organic carbon in the ocean with the model's soft biogenic material, measurements of particulate organic carbon may help to constrain strongly the relative magnitude of β_2 and β_{-2}.

The cycle of soft biogenic material through the model's water column differs in important ways from the cycles of thorium and total particulate material. The only source of soft biogenic mate-

rial is the euphotic zone; in contrast, there are parent nuclides throughout the water column for the thorium isotopes (except ^{232}Th). Unlike soft biogenic material, hard biogenic material and inert particulate material are not subject to remineralization through the water column. As a result of these differences, predicted profiles of soft biogenic material are sensitive to the magnitude of β_2 and β_{-2}. These results imply that by combining measurements of particulate organic carbon (POC), particulate organic nitrogen (PON), thorium, and particle mass one could obtain more precise estimates of β_2 and β_{-2}.

It is important to remember that these profiles are produced by a one-dimensional steady state model. Advective and diffusive transport and non-steady state conditions make distinguishing different rates more difficult. The uncertainty in T( ) will act to limit the precision with which the rate constants can be determined.

Summary

We use an inversion technique (TV) to calculate least squares estimates for the rate of particle and thorium cycling through the water column at the Nares Abyssal Plain. The data used in the inversion combines results from adjacent stations that were occupied at different times (GEOSECS, TTO-NAS, *Cochran et al* [1987], *Fisher et al.* [1988]). Initial estimates of the time dependence and transport terms were assumed to sum to zero (T( ) = 0). The predicted values for T( ) were nonzero and on the same order as other terms in the conservation equations for thorium and particles. Most of the predicted rate constants related to particle cycling (β_{-1}, β_2, and β_{-2}) have large uncertainties and differ from their initial estimates by less than 30% (Table 4). Estimated median values for the aggregation rate (2.1-3.6 y^{-1}) and disaggregation rate (135-195 y^{-1}) of particles are within the range of previous estimates (Table 1). Predicted median values for β_{-1} range from a high of 75 y^{-1} in the euphotic zone to a low of 0.2 y^{-1} at the bottom level in the model. The large errors in the rate constants show that the data set does not strongly constrain the particle-cycling rate constants. The rate constants for thorium adsorption and desorption are better constrained by the data. The mean value for the predicted adsorption rate constant is $5.0\pm1.0\times10^4$ m^3 kg^{-1} y^{-1} and for the desorption rate constant is 3.1 ± 1.5 y^{-1}.

An analysis, based on the inversion results, of the relative magnitude of the processes involved in the cycling of thorium and particles through the water column shows that the sum of the time dependence and lateral transport terms, T( ), can be on the same order as, or greater than, other terms in the conservation equations for particle and thorium cycling in the northwest Atlantic Ocean. Large errors for the rate constants predicted with the inversion are related to the uncertainties in the values of T( ) and the insensitivity of thorium and total particle profiles to parallel changes in β_{-2} and β_2. The inversion results suggest that until the uncertainty and value of T( ) is included in calculations, the predicted error and the estimated range of the rate constants will remain large. More detailed sampling, estimates of time rates of change, and estimates of lateral and vertical transport parameters will be needed to constrain the rate constants, certainly a nontrivial task.

Particle and thorium profiles are predicted with a forward model of particle and thorium cycling using rate constants predicted with the inversion technique. Sensitivity tests made with the forward model show that for a given ratio of β_2/β_{-2}, different values for β_2 and β_{-2} cannot be distinguished using thorium activity profiles except where there are rapidly changing particle and thorium flux gradients. The concentration and flux of soft biogenic material in the forward model, however, are quite sensitive to changes in β_2 and β_{-2} for a given ratio of β_2/β_{-2}. Measurements of the distribution and flux of soft biogenic material (e.g., particulate organic carbon, nitrogen, and phosphorus) may provide the best chance to determine β_2 and β_{-2} with some precision. The data collected by the Joint Global Ocean Flux Study (JGOFS) expeditions (e.g., thorium, POC, and PON data summarized from the North Atlantic Bloom experiment [*Buesseler et al.*, 1992]) will provide the information needed to determine T( ) and should allow the rate constants to be determined with relatively good precision.

Appendix A. Particle and Thorium Model Equations

As noted in the text, the conservation equations for thorium and particles can be written as SMS( ) = T( ), where SMS( ) includes all the source minus sink terms and T( ) represents the advective and diffusive transport and the time rate of change. The conservation equations describing the thorium model in Figure 1 can be expanded as

Dissolved phase, A_D

$$A_S(P^t_S k_{-1} + P^s_S\beta_{-1}) - A_D(P^t_S k_1 + \lambda) + A_P\lambda = T(A_D) \quad \text{(A1a)}$$

Small-particle phase, $A_S P^t_S$

$$A_D P^t_S k_1 + A_L P^t_L \beta_{-2} - A_S(P^t_S(k_{-1} + \beta_2 + \lambda) + P^s_S\beta_{-1}) = T(A_S P^t_S) \quad \text{(A1b)}$$

Large-particle phase, $A_L P^t_L$

$$A_S P^t_S\beta_2 - A_L P^t_L(\beta_{-2} + \lambda) - \omega\frac{\partial A_L P^t_L}{\partial z} = T(A_L P^t_L) \quad \text{(A1c)}$$

where the term T( ) represents

$$T(\,) = \frac{\partial(\,)}{\partial t} + \vec{\mathbf{V}}\bullet\vec{\nabla}(\,) - \vec{\nabla}\bullet\mathbf{K}\vec{\nabla}(\,) \quad \text{(A1d)}$$

and the blank space in T( ) is filled by the appropriate term for each equation. The conservation equations for the particles can be expanded as

Nutrient phase, N

$$P^s_S\beta_{-1}R^s - N\beta_1 = T(N) \quad \text{(A2a)}$$

Soft biogenic small-particle phase, P^s_S

$$P^s_L\beta_{-2} + \frac{N\beta_1}{R^s} - P^s_S(\beta_2 + \beta_{-1}) = T(P^s_S) \quad \text{(A2b)}$$

Hard biogenic small-particle phase, P^h_S

$$P^h_L\beta_{-2} + \frac{N\beta_1}{R^h} - P^h_S\beta_2 = T(P^h_S) \quad \text{(A2c)}$$

Inert detrital small-particle phase, P^i_S

$$P^i_L\beta_{-2} - P^i_S\beta_2 = T(P^i_S) \quad \text{(A2d)}$$

Large-particle phase, P^*_L

$$P^*_S\beta_2 - P^*_L\beta_{-2} - \omega\frac{\partial P^*_L}{\partial z} = T(P^*_L) \quad \text{(A2e)}$$

Activity is denoted by A and the subscripts D, S, and L show activity in the dissolved, small-particle, and large-particle classes. The A_P denotes the activity of the dissolved thorium parent. The dissolved thorium activity is in disintegrations per minute per cubic meter, and the small and large thorium particle activities are in disintegrations per minute per kilogram. The processes denoted by the different rates are depicted in Figure 1. The units for k_{-1}, λ, β_1, β_2, β_{-1}, and β_{-2} are per year. The units for k_1 are cubic meter per kilogram per year. The ratio of particulate nutrient to mass of soft biogenic material is given by R^s, and the ratio of particulate nutrient to hard biogenic material is given by R^h. Advective velocity is given by **V**, eddy diffusivity by **K**, time by t, and depth by z. Particle concentrations, P, are given in kilograms per cubic meter. The subscripts to P mark the small, S, or large, L, particle phase, and the superscripts mark the soft biogenic material, s, hard biogenic material, h, inert detrital material, i, or the total mass in a given particle class, t. The asterisk in (A2c) symbolizes s, h, or i. The flux of large particles can be related to the large-particle concentration: $P_L\omega = F_{P_L}$.

Equations A1 and A2 were changed slightly for use as constraint equations in the inversion. All of the rate constants, ω, and the small and large soft biogenic particle concentrations were assumed to have a lognormal probability distribution. The change in the conservation equations resulted in the following equations for (A1):

Dissolved phase, A_D

$$A_S((P^i_S + P^h_S + exp(\ln(P^s_S)))exp(\ln(k_{-1})) + exp(\ln(P^s_S))exp(\ln(\beta_{-1}))) - A_D((P^i_S + P^h_S + exp(\ln(P^s_S)))exp(\ln(k_1)) + \lambda) + A_P\lambda = T(A_D) \quad \text{(A3a)}$$

Small-particle phase, $A_SP^t_S$

$$A_D(P^i_S + P^h_S + exp(\ln(P^s_S)))exp(\ln(k_1)) + A_L(P^i_L + P^h_L + exp(\ln(P^s_L)))exp(\ln(\beta_{-2})) - A_S((P^i_S + P^h_S + exp(\ln(P^s_S)))(exp(\ln(k_{-1})) + exp(\ln(\beta_2)) + \lambda) + exp(\ln(P^s_S))exp(\ln(\beta_{-1}))) = T(A_SP^t_S) \quad \text{(A3b)}$$

Large-particle phase, $A_LP^t_L$

$$A_S(P^i_S + P^h_S + exp(\ln(P^s_S)))exp(\ln(\beta_2)) - A_L(P^i_L + P^h_L + exp(\ln(P^s_L)))exp(\ln(\beta_{-2})) + \lambda) - exp(\ln(\omega))\frac{\partial A_L(P^i_L + P^h_L + exp(\ln(P^s_L)))}{\partial z} = T(A_LP^t_L) \quad \text{(A3c)}$$

The soft biogenic material conservation equations were altered in a similar manner:

Soft biogenic small-particle phase, P^s_S

$$exp(\ln(P^s_L))exp(\ln(\beta_{-2})) + \frac{Nexp(\ln(\beta_1))}{exp(\ln(R^s))} - exp(\ln(P^s_S))(exp(\ln(\beta_2)) + exp(\ln(\beta_{-1}))) = T(P^s_S) \quad \text{(A4a)}$$

Large-particle phase, P^*_L

$$exp(\ln(P^s_S))exp(\ln(\beta_2)) - exp(\ln(P^s_L))exp(\ln(\beta_{-2})) - exp(\ln(\omega))\frac{\partial exp(\ln(P^s_L))}{\partial z} = T(P^*_L) \quad \text{(A4b)}$$

Equations A3 for thorium and A4 for soft biogenic material are used as constraint equations in the inversion of the particle and thorium data for the 13 depths of the water column. The equations are nonlinear so that initial estimates for all the terms that will be optimized in a least squares sense are required. The methods used to obtain the initial estimates are given in Appendix B.

A one-dimensional, steady state forward model of particle and thorium cycling that predicts particle and thorium concentrations and fluxes through the water column can be constructed using the rate constants predicted with the inversion. The steady state forward model lacks advective and diffusive terms so that T( ) equals zero as in the initial estimates for the inversion. The particle- and thorium-cycling equations can be applied throughout the water column. Each point is coupled to adjacent points by sinking large particles. Thorium activities and particle concentrations at each point could be calculated with a finite difference model; however, it is much more efficient to directly solve a system of linear equations. The particle concentrations must be known before the thorium equations can be solved; therefore the particle concentrations are solved first. The particle equations for the forward model are based on (A2) and the inversion results, but T( ) = 0 and the production of small particles in the euphotic zone are on the right-hand side. The linear equations for particles at a given level are

$$\begin{pmatrix} -(\beta_{-1}(i)+\beta_2(i)) & 0 & \beta_{-2}(i) \\ \beta_2(i) & \frac{\omega}{\Delta z(i)} & -(\beta_{-2}(i)+\frac{\omega}{\Delta z(i)}) \end{pmatrix} \begin{pmatrix} P^s_S(i) \\ P^s_L(i-1) \\ P^s_L(i) \end{pmatrix} = \begin{pmatrix} \{-[PO^{3-}_4]\beta_1(i)(R^s)^{-1}\ ;\ 0<i\le 2 \\ 0\ ;\ 2<i \} \\ 0 \end{pmatrix} \quad \text{(A3)}$$

where i is an index for the layer in the model. The large-particle concentration of soft biogenic material is set equal to zero at the air-sea interface (at i=0). The elements in the unknown vector for the forward model are the small- and large-particle concentrations at each depth. The euphotic zone comprises the top two layers where there is a particle production term. The phosphate concentrations at GEOSECS station 31 are used for the nutrient concentration. The Δz term represents the layer thickness. The system of equations can be solved for all levels at one time. Once the soft biogenic particle concentrations are known, a similar technique can be used to find the activities for the different thorium isotopes using (A1). The appropriate equation is

$$\begin{pmatrix} \alpha_{11} & \alpha_{12} & 0 & 0 \\ P^t_S(i)k_1 & \alpha_{22} & 0 & P^t_L(i)\beta_{-2}(i) \\ 0 & P^t_S(i) & \frac{\omega}{\Delta z(i)} & \alpha_{34} \end{pmatrix} \begin{pmatrix} A_D(i) \\ A_S(i) \\ A_L(i-1) \\ A_L(i) \end{pmatrix} = \begin{pmatrix} -A_P(i)\lambda \\ 0 \\ 0 \end{pmatrix} \quad \text{(A4)}$$

where

$$\alpha_{11} = -P^t_S(i)k_{-1} - \lambda$$

$$\alpha_{12} = P^s_S(i)\beta_{-1}(i) + P^t_S(i)k_{-1}$$

$$\alpha_{22} = -P^t_S(i)(k_{-1} + \beta_2(i) + \lambda) - P^s_S(i)\beta_{-1}(i)$$

$$\alpha_{34} = -P^t_L(i)(\beta_{-2}(i) + \lambda + \frac{\omega}{\Delta z(i)})$$

All the terms in (A4) are defined above. Solving these equations for every level in the model yields the activities and fluxes based on the rates and settling velocity predicted with the inversion applied to a situation where T( ) = 0 in (A1) and (A2). The predicted profiles will differ from those found with the inversion because the inversion solution has T( ) ≠ 0.

Appendix B: Field Data and Initial Estimates

Samples for measurements of ^{230}Th and ^{228}Th in solution and on suspended particles were collected in September 1984 at a site in the Nares Abyssal Plain (23°11'N, 63°58'W) [*Cochran et al.*, 1987]. Figure 2 shows the measured activities of ^{228}Th and ^{230}Th in the suspended particles and in solution. No ^{228}Ra measurements were made when samples were collected for ^{228}Th, and we have used ^{228}Ra analyses on samples collected in 1981 as part of the TTO-NAS (station 24, 23°17'N, 64°09'W [*Key et al.*, 1992]). The ^{228}Ra activities that were measured from the TTO samples are shown in Figure 2. The interpolated thorium and radium activities are listed in Table 2 and a curve connecting the values is shown in Figure 2.

Our approach is in the spirit of *Wunsch*'s [1984] eclectic approach: we try to include a wide variety of relevant data into an inverse solution. With this in mind we use several numbers (specifically uranium activities and ^{234}Th activities) that are not directly measured but that are expected to be correct. Depth-invariant uranium activities of 2.8×10^3 dpm ^{234}U m^{-3} and 2.4×10^3 dpm ^{238}U m^{-3} were used in the model. No measurements of ^{234}Th were made at the Nares Abyssal Plain site. This short-lived thorium isotope commonly shows a depletion relative to its parent ^{238}U in the upper ≈100 m [e.g., *Coale and Bruland*, 1985, 1987], but at depth it is close to equilibrium with dissolved ^{238}U. In order to provide additional constraints based on thorium isotopes for the model and because of the relatively predictable ^{234}Th activities we include equations for ^{234}Th below level four in the inversion. On the basis of other studies [*Bacon and Anderson*, 1982; *Buesseler et al.*, 1992] we assume that ≈4% of the total ^{234}Th activity is present on suspended particles below 220 m (level 4 and below) so that the initial activity of dissolved ^{234}Th is 2.3×10^3 dpm m^{-3} (Table 2).

The distribution of the total concentration of suspended particles at the Nares site is obtained from GEOSECS measurements (station 31; 27°N, 53°32'W). Figure 3 shows the suspended particle data and the curve connecting the interpolated values (Table 3) derived for the model layers.

Mass fluxes of particles and thorium isotopes are obtained from a 1-y (1984) deployment of two sediment traps (1464 m and 4832 m) at the Nares site [*Fisher et al.*, 1988]. Mean annual fluxes of ^{230}Th and ^{228}Th determined from the two traps are used in the model. A complete profile of particle flux with depth was produced using these data and the mass flux compilation of *Hargrave* [1985] for the northwest Atlantic. The Nares site is one of low productivity, and the measured fluxes are at the lower end of the regional averages compiled by *Hargrave* [1985]. We use Hargrave's compilation to determine the shape of the flux profile. We use the low end of the estimated ranges [*Hargrave*, 1985] and the mean annual fluxes directly measured at Nares. The interpolated fluxes are listed in Table 3 and the curve running through the interpolated values is shown in Figure 3.

The initial estimates for terms that were not measured (besides the uranium isotopes and ^{234}Th activities) are based on the assumptions that the system is at steady state, that lateral transport is negligible, and that the settling of large particles is the only significant vertical transport term; in other words, T( ) = 0. The validity of these assumptions is examined in the main text. The uncertainty for T( ) is a function of the initial estimates for the terms in SMS( ). The standard deviation for T( ) equals 10 times the value of SMS( ) calculated with the initial estimates except for the soft biogenic material equations where a value of 0.01 kg m^{-3} y^{-1} was used.

The initial estimate for the large-particle settling velocity, ω, was set at 150±100 m d^{-1}. The total large-particle concentration at depth ($1.9\pm1.3\times10^{-7}$ kg m^{-3}) is based on a settling velocity of 150 m d^{-1}, the average mass flux at 1464 m and 4832 m at the Nares Abyssal Plain measured by *Fisher et al.* [1988], and error propagation of the average mass flux and the settling velocity error. The depth-weighted average of the small-particle concentration between 1464 and 4832 m (found with the GEOSECS data) is $11.2\pm0.5\times10^{-6}$ kg m^{-3}. Using these values, the assumptions that the large-particle flux gradient and T( ) equal zero, and (A2e) for the total large particles, we find the relation

$$\beta_2 = 1.65\pm1.16\times10^{-2}\beta_{-2}$$

The depth-weighted small-particle ^{230}Th activity is $6.8\pm0.3\times10^{-2}$ dpm m^{-3}; however, when this value is used in the calculations, a negative value is found for β_{-2}. Therefore the small-particle ^{230}Th activity for level 11 (at 3721 m) was omitted from the depth average because its low value (Figure 2) departs from the monotonic increase expected for one-dimensional steady state conditions. The resultant depth-averaged small-particle ^{230}Th activity between the sediment traps is $7.9\pm0.4\times10^{-2}$ dpm m^{-3} [*Cochran et al.*, 1987], the average large-particle ^{230}Th activity is $6.35\pm2.80\times10^3$ dpm kg^{-1}, and the ^{230}Th flux gradient is $2.0\pm1.3\times10^{-2}$ dpm m^{-3} y^{-1} [*Fisher et al.*, 1988]. Using (A1c), the assumption that T( ) for large-particle ^{230}Th is zero, error propagation, and the previous relation between β_2 and β_{-2}, we find that $\beta_{-2} = 155\pm1610$ y^{-1} and that $\beta_2 = 3\pm27$ y^{-1}. These values were used throughout the water column as the initial guesses for β_{-2} and β_2.

The dissolved thorium and ^{228}Ra activities are based on the interpolated data (Table 2) and assigned uncertainties of ±10%. Unless explicitly stated otherwise, the errors given to the remaining terms are based on error propagation and the uncertainties given above for β_2 and β_{-2}, thorium activities and fluxes, and the large-particle settling velocity and total large-particle fluxes.

The initial estimate for R^s, the ratio of particulate nutrient particle mass, is based on a C/P Redfield ratio of 130 [*Peng and Broecker*, 1987] and the following relation:

$$R^s = \frac{1 \text{ mol phosphate}}{(CH_2O)_{130}(NH_3)_{16}(H_3PO_4)} = 0.234 \text{ mol kg}^{-1}$$

The initial estimate of R^s agrees with field observations. Data from *Collier and Edmond* [1984] can be used to find independent estimates of R^s. *Collier and Edmond* [1984] list millimole per gram dry plankton values of Ca, Si, and P from a variety of ocean stations. If we assume that one mole of Ca gives 0.1 kg of $CaCO_3$ and that one mole of Si gives 0.062 kg of SiO_2 that is 10% water, then we can estimate values of R^s that range from 0.1 mol kg^{-1} in the Antarctic Ocean to 0.7 mol kg^{-1} in the equatorial Pacific (Manganese Nodule Project (MANOP) site C). Another check can be made using data from *Parsons et al.* [1961] who give a dry weight to C (grams) ratio of 2.5. Using a C/P ratio of 130, this is equivalent to a mole P/kilogram dry weight ratio of 0.26. A final comparison is made using data from *Jackson* [1990]. *Jackson* [1990] finds 2.2×10^{-6} g C in a 1 mm diameter aggregate and,

using data from *Alldredge and Gotschalk* [1988] (1 mm aggregate has 1×10^{-5} g dry weight), calculates a dry weight to C ratio of 4.5. This is equivalent to a mole P/kilogram dry weight ratio of 0.14. All of these values are within a factor of 4 of our initial estimate for R^s, 0.234, and we assign to this number a large error of ±0.468.

We next find the values for the particle concentrations based on the measured data. The flux of soft biogenic material is based on the average ($502\pm158\times10^{-6}$ kg C m^{-2} y^{-1}) of the measured organic carbon fluxes at Nares [*Fisher et al.*, 1988]. Using a molar C/P ratio of 130 and the estimate of R^s, we find that the flux of soft biogenic material is $1.37\pm0.43\times10^{-3}$ kg m^{-2} y^{-1}. We also assume that 60% of the flux of material at Nares is from hard biogenic material (e.g., calcite and opal) to get a flux of $6.06\pm1.56\times10^{-3}$ kg m^{-2} y^{-1}. The 60% value is not unreasonable when compared to other sediment trap data [*Brewer et al.*, 1980; *Deuser et al.*, 1981; *Honjo et al.*, 1982; *Deuser*, 1986], and in any case, it does not strongly influence the rate constant solutions. Subtracting the flux of biogenic material from the total flux of particulate material gives the flux of inert abiogenic material, $2.67\pm3.06\times10^{-3}$ kg m^{-2} y^{-1}. Dividing the fluxes of inert abiogenic material and hard biogenic material by the settling velocity gives us the large-particle concentrations of inert abiogenic material ($4.9\pm6.5\times10^{-8}$ kg m^{-3}) and hard biogenic material ($1.1\pm0.8\times10^{-7}$ kg m^{-3}). Subtracting these two values from the total large-particle concentration gives the large-particle concentration of soft biogenic material ($0.3\pm1.7\times10^{-7}$ kg m^{-3}).

The particle concentrations for the various phases at different depths through the water column were found as follows: The flux of inert abiogenic particles was assumed to be constant through the water column; therefore the initial estimate for the concentration was the same throughout the water column. The flux of hard biogenic material was assumed to be constant below the euphotic zone; therefore the initial estimate for the hard biogenic large-particle concentration was the same below the euphotic zone. The concentration was assumed to decrease linearly from this concentration at the base of the euphotic zone to zero at the surface. The large-particle concentration of soft biogenic particles was found by subtracting the large-particle concentrations of inert abiogenic and hard biogenic particles (see Table 3) from the total large-particle concentration (based on the interpolated total fluxes (Table 3) divided by the settling velocity). The total particle flux was assumed to have an uncertainty of 50% for error propagation calculations.

The small-particle concentrations of hard biogenic and inert abiogenic material was found using the relation $P_S = P_L\beta_{-2}/\beta_2$ and using the appropriate P_L concentrations. This relation is based on (A2d). The small-particle concentration of soft biogenic material is found through the relation given by (A2e). At some levels, negative concentrations are calculated because of a large negative gradient in the large-particle concentration of soft biogenic material. For the cases where negative estimates were found the concentration of soft biogenic material in the overlying layer was used.

The initial estimate for β_1 is based on an assumed primary productivity at Nares Abyssal Plain of 0.04 kg C m^{-2} y^{-1} [*Berger*, 1989] and interpolated phosphate concentrations in the euphotic zone based on GEOSECS data. We assign an uncertainty of 50% to this estimate of primary production. The relation between nutrients, primary production (PP), and β_1 is given by

$$\beta_1 = \frac{PP}{12\times130\times PO_4\times\Delta z}$$

where Δz is the thickness of the given layer in the euphotic zone.

The values for β_{-1} through the water column are found using (A2b) where $\beta_1 = 0$ below the euphotic zone and the initial estimates for β_{-2} and β_2. After calculating β_{-1} through the water column any negative values for β_{-1} were replaced by the average of the nearest positive β_{-1} above and below the given layer. The uncertainty found by error propagation was retained.

The rates of thorium adsorption and desorption must also be estimated. The rate constant for k_1 is set equal to 5×10^4 m^3 kg^{-1} y^{-1}. This is equivalent to a $k_1' = k_1\times P_S^s = 0.5$ y^{-1} when the small-particle concentration is 1×10^{-5} kg m^{-3} and is within the range of many field estimates for k_1' (Table 1). The initial estimate for k_{-1} equals 3 y^{-1} and is in the middle of estimates listed in Table 1. The value for k_{-1} is independent of particle concentration. The initial standard deviations for both rate constants are set equal to their value in order to span the range listed in Table 1. The smaller error relative to the β's is warranted because adsorption and desorption rates are better known.

Lavelle et al. [1991] used estimates for k_{-1} that are several orders of magnitude greater than most field-based values (Table 1) in order to maintain K_D values that agree with laboratory data. This caused their values for k_1 to be on the high end of field-based estimates. The lower values for k_{-1} that are found in the ocean could be due to differences between processes occurring in the ocean and the in lab.

Small-particle thorium activities in disintegrations per minute per kilogram are calculated from the interpolated activities in Figure 2 (and listed in Table 2) and the interpolated total small-particle concentration (Figure 3). The uncertainties for the activities are based on 10% uncertainties in the interpolated values of small-particle thorium activities in disintegrations per minute per cubic meter and of the total small-particle concentrations.

The remaining terms that require initial estimates are the large-particle thorium activities. *Clegg and Whitfield* [1991] predict the variation in activity of the small- and large-particle phases as a function of the rate constants β_2 and β_{-2}. A general estimate based on their work for the large-particle ^{234}Th and ^{230}Th activities (in disintegrations per minute per kilogram) is that the large-particle activities equal 80% of the small-particle activities (in disintegrations per minute per kilogram). Estimates for the ^{230}Th and ^{228}Th large-particle thorium activity can also be found using flux data [*Fisher et al.*, 1988]. The large-particle ^{230}Th activity is very close to 80% of the small-particle ^{230}Th activity [*Cochran et al.*, 1987], which agrees with the work of *Clegg and Whitfield* [1991]. Therefore the initial estimates of ^{234}Th and ^{230}Th large-particle activities are set equal to 0.8 times the small-particle activities (Table 2) with an uncertainty of ±20%. The relationship of large-particle to small-particle ^{228}Th activity is more complicated. The ratio of large- to small-particle ^{228}Th activities near the ocean surface and bottom tend to be less than one because of the greater activity of the parent nuclide ^{228}Ra. At intermediate depths the ratio of large- to small-particle ^{228}Th activity is greater than one. The large- to small-particle ^{228}Th activity ratio varies widely between the two sediment traps: 3.6 at the 1464 m trap and 1.6 at the 4832 m trap. On the basis of the results of *Clegg and Whitfield* [1991] the large- to small-particle ^{228}Th activity should drop below one near the surface. Therefore the large- to small-particle ^{228}Th activity ratio at level 3 is set equal to one. Linear interpolation between these three values is used to find the activity ratios at each depth (Table 2). The greater uncertainty associated with estimating the large-particle thorium activity is accounted for by assigning an uncertainty of ±50% to the large-particle ^{228}Th activity.

When carrying out the inversion, the terms that are assumed to have lognormal distributions must still be transformed. Therefore the log was taken of the initial estimates for the small- and large-particle soft biogenic material concentration, all the rate constants, the settling velocity, and R^s. The standard deviation of the transformed values (σ) was found from the relation

$$\sigma = \ln\left(\frac{x + \sigma^*}{x}\right)$$

where x represents the untransformed term and σ^* is the standard deviation of the untransformed variable.

The antilog of the least squares solution of the transformed variables gives the median of the lognormal distribution. The antilog of the sum of the least squares solution plus or minus the standard deviation does not give any statistically significant value; however, it does provide an easy comparison to the variables with normal distributions. The mean and standard deviation of the lognormal distribution can be calculated using the least squares solution for the normal distribution [*Aitchison and Brown*, 1966]. The standard deviation of the lognormal distribution gives a measure of the spread in the tail of the lognormal distribution and does not directly parallel the standard deviation of a normal distribution. In addition, the nonlinear system precludes the rigorous calculation of a covariance matrix. Because of these complications we present the solution in two ways: (1) a minimum variance unbiased estimate of the mean and standard deviation of the lognormal distribution, and (2) the antilog of the mean and the antilog of the sum of the mean plus/minus the standard deviation of the normal distribution.

Note that the equations for the thorium isotopes were scaled such that the activity of each isotope was of the same order. This prevents the ^{234}Th equations from dominating the solution with respect to the ^{230}Th and ^{228}Th equations. The ^{230}Th equations were multiplied by 10^4 and the ^{228}Th equations were multiplied by 10^2. In addition, the only conservation equations for particle cycling directly included in the inversion were for the cycling of soft biogenic material in the large- and small-particle phases.

Acknowledgments. Portions of this work were completed while JKC was a visiting fellow in the Program in Atmospheric and Oceanic Sciences at Princeton University. This work was supported by grants from the National Science Foundation (OCE88-19544 and OCE90-16832) to JKC and (OCE90-12333) to JLS, and from the Department of Energy (DE-FG02-90ERG1052) to JLS. This is contribution 905 from the Marine Sciences Research Center.

References

Aitchison, J., and J. A. C. Brown, *The Lognormal Distribution With Special Reference to Its Uses in Economics*, 176 pp., Cambridge University Press, New York, 1966.

Alldredge, A. L., and C. Gotschalk, In situ settling behavior of marine snow, *Limnol. Oceanogr.*, *33*, 339-351, 1988.

Anderson, R. F., M. P. Bacon, and P. G. Brewer, Removal of ^{230}Th and ^{231}Pa at ocean margins, *Earth Planet. Sci. Lett.*, *62*, 7-23, 1983.

Bacon, M. P., Radionuclide fluxes in the ocean interior, in *Global Ocean Flux Study, Proceedings of a Workshop*, pp.180-205, Board on Ocean Science and Policy, National Research Council, National Academy Press, Washington, D.C., 1984.

Bacon, M. P., and R. F. Anderson, Distribution of thorium isotopes between dissolved and particulate forms in the deep sea, *J. Geophys. Res.*, *87*, 2045-2056, 1982.

Bacon, M. P., C.-A. Huh, A. P. Fleer, and W. G. Deuser, Seasonality in the flux of natural radionuclides and plutonium in the deep Sargasso Sea, *Deep Sea Res., Part A*, *32*, 273-286, 1985.

Bacon, M. P., C. A. Huh, and R. M. Moore, Vertical profiles of some natural radionuclides over the Alpha Ridge, Arctic Ocean, *Earth Planet. Sci. Lett.*, *95*, 15-22, 1989.

Berger, W. H., Global maps of ocean productivity, in *Productivity of the Ocean: Present and Past*, edited by W. H. Berger, V. S. Smetacek, and G. Wefer, pp.471, John Wiley, New York, 1989.

Brewer, P. G., Y. Nozaki, D. W. Spencer, and A. P. Fleer, Sediment trap experiments in the deep North Atlantic: Isotopic and elemental fluxes, *J. Mar. Res.*, *38*, 703-728, 1980.

Buesseler, K. O., Do upper-ocean sediment traps provides an accurate record of particle flux?, *Nature*, *353*, 420-423, 1991.

Buesseler, K. O., M. P. Bacon, J. K. Cochran, and H. D. Livingston, Carbon and nitrogen export during the JGOFS North Atlantic Bloom Experiment estimated from ^{234}Th:^{238}U disequilibria, *Deep Sea Res., Part A*, *39*, 1115-1138, 1992.

Clegg, S. L., and M. Whitfield, A generalized model for the scavenging of trace metals in the open ocean, I, Particle cycling, *Deep Sea Res.*, *37*, 809-832, 1990.

Clegg, S. L., and M. Whitfield, A generalized model for the scavenging of trace metals in the open ocean, II, Thorium scavenging, *Deep Sea Res., Part A*, *38*, 91-120, 1991.

Clegg, S. L., M. P. Bacon, and M. Whitfield, Application of a generalized scavenging model to thorium isotope and particle data at Equatorial and high-latitude sites in the Pacific Ocean, *J. Geophys. Res.*, *96*, 20655-20670, 1991.

Coale, K. H., and K. W. Bruland, ^{234}Th:^{238}U disequilibria within the California Current, *Limnol. Oceanogr.*, *30*, 22-33, 1985.

Coale, K. H., and K. W. Bruland, Oceanic stratified euphotic zone as elucidated by ^{234}Th:^{238}U disequilibria, *Limnol. Oceanogr.*, *32*, 189-200, 1987.

Cochran, J. K., H. D. Livingston, D. J. Hirschberg, and L. D. Surprenant, Natural and anthropogenic radionuclide distributions in the northwest Atlantic, *Earth Planet. Sci. Lett.*, *84*, 135-152, 1987.

Collier, R., and J. Edmond, The trace element geochemistry of marine biogenic particulate matter, *Prog. Oceanogr.*, *13*, 113-199, 1984.

Deuser, W. G., Seasonal and interannual variations in deep-water particle fluxes in the Sargasso Sea and their relation to surface hydrography, *Deep Sea Res., Part A*, *33*, 225-246, 1986.

Deuser, W. G., E. H. Ross, and R. F. Anderson, Seasonality in the supply of sediment to the deep Sargasso Sea and implications for the rapid transfer of matter to the deep ocean, *Deep Sea Res., Part A*, *28*, 495-505, 1981.

Deuser, W. G., F. E. Muller-Karger, R. H. Evans, O. B. Brown, W. E. Esaias, and G. C. Feldman, Surface-ocean color and deep-ocean carbon: How close a connection?, *Deep Sea Res., Part A*, *37*, 1331-1343, 1990.

Eppley, R. W., New Production: History, methods, problems, in *Productivity of the Ocean: Present and Past*, edited by W. H. Berger, V. S. Smetacek, and G. Wefer, pp.85-97, John Wiley, New York, 1989.

Fisher, N. S., P. Bjerregaard, and S. W. Fowler, Interactions of marine plankton with transuranic elements, 1, Biokinetics of neptunium, plutonium, americium, and californium in phytoplankton, *Limnol. Oceanogr.*, *28*, 432-447, 1983.

Fisher, N. S., M. Bohe, and J.-L. Teyssie, Accumulation and toxicity of Cd, Zn, Ag, and Hg in four marine phytoplankters, *Mar. Ecol. Prog. Ser.*, *18*, 201-213, 1984.

Fisher, N. S., J. K. Cochran, S. Krishnaswami, and H. D. Livingston, Predicting the oceanic flux of radionuclides on sinking biogenic debris, *Nature*, *335*, 622-625, 1988.

Hargrave, B. T., Particle sedimentation in the ocean, *Ecol. Model.*, *30*, 229-246, 1985.

Honeyman, B. D., and P. H. Santschi, A Brownian-pumping model for oceanic trace metal scavenging: Evidence from Th isotopes, *J. Mar. Res.*, *47*, 951-992, 1989.

Honjo, S., S. J. Manganini, and J. J. Cole, Sedimentation of biogenic matter in the deep ocean, *Deep Sea Res., Part A*, *29*, 609-625, 1982.

Jackson, G. A., A model of the formation of marine algal flocs by physical coagulation processes, *Deep Sea Res., Part A, 37*, 1197-1211, 1990.

Jannasch, H. W., B. D. Honeyman, L. S. Balistrieri, and J. W. Murray, Kinetics of trace element uptake by marine particles, *Geochim. Cosmochim. Acta, 52*, 567-577, 1988.

Key, R. M., J. L. Sarmiento, and W. S. Moore, Transient tracers in the ocean North Atlantic Study, Final data report for ^{228}Ra and ^{226}Ra, *Tech. Rep., 92-2*, Ocean Tracer Lab., Princeton Univ., Princeton, N. J., 1992.

Lavelle, J. W., C. N. Cudaback, A. J. Paulson, and J. W. Murray, A rate for the scavenging of fine particles by macroaggregates in a deep estuary, *J. Geophys. Res., 96*, 783-790, 1991.

Menke, W., *Geophysical Data Analysis: Discrete Inverse Theory*, 260 pp., Academic, San Diego, Calif., 1984.

Moore, R. M., and G. E. Millward, The kinetics of reversible Th reactions with marine particles, *Geochim. Cosmochim. Acta, 52*, 113-118, 1988.

Murnane, R. J., Determination of thorium and particulate matter cycling parameters at station P: A reanalysis and comparison of least squares techniques, *J. Geophys. Res., in press*, 1993a.

Murnane, R. J., Determining thorium and particle cycling rates using least squares techniques, *Tech. Rep.*, Ocean Tracer Lab., Princeton Univ., Princeton, N.J., 1993.

Murnane, R. J., J. L. Sarmiento, and M. P. Bacon, Thorium isotopes, particle cycling models, and inverse calculations of model rate constants, *J. Geophys. Res., 95*, 16,195-16,206, 1990.

Najjar, R. G., J. L. Sarmiento, and J. R. Toggweiler, Downward transport and fate of organic matter in the oceans: Simulations with a general circulation model, *Global Biogeochem. Cycles, 6*, 45-76, 1992.

Nozaki, Y., Y. Horibe, and H. Tsubota, The water column distributions of thorium isotopes in the western North Pacific, *Earth Planet. Sci. Lett., 54*, 203-216, 1981.

Nozaki, Y., J. S. Yang, and M. Yamada, Scavenging of thorium in the ocean, *J. Geophys. Res., 92*, 772-778, 1987.

Parsons, T. R., K. Stephens, and J. D. H. Strickland, On the chemical composition of eleven species of marine phytoplankters, *J. Fish. Res. Board Can., 18*, 1001-1016, 1961.

Peng, T.-S., and W. S. Broecker, C/P ratios in marine sediments, *Global Biogeochem. Cycles, 1*, 155-161, 1987.

Rothschild, V., and N. Logothetis, *Probability Distributions*, 70 pp., Wiley, New York, 1986.

Siegel, D. A., T. C. Granata, A. F. Michaels, and T. D. Dickey, Mesoscale eddy diffusion, particle sinking, and the interpretation of sediment trap data, *J. Geophys. Res., 95*, 5305-5311, 1990.

Tarantola, A., and B. Valette, Generalized nonlinear inverse problems solved using the least squares criterion, *Rev. Geophys., 20*, 219-232, 1982.

Wunsch, C., An eclectic Antlantic Ocean circulation model, I, The meridional flux of heat, *J. Phys. Oceanogr., 14*, 1712-1733, 1984.

J. K. Cochran, Marine Sciences Research Center, State University of New York at Stony Brook, Stony Brook, NY 11794.

R. J. Murnane and J. L. Sarmiento, Program in Atmospheric and Oceanic Sciences, Princeton University, Princeton, NJ 08544. (e-mail: murnane@splash.princeton.edu)

(Received July 22, 1993; revised August 23, 1993;
accepted August 23, 1993.)